Hindawi
International Journal of Energy Research
Volume 2024, Article ID 7939416, 25 pages
https://doi.org/10.1155/2024/7939416

Research Article

Cascaded Fractional-Order Controller-Based Load Frequency Regulation for Diverse Multigeneration Sources Incorporated with Nuclear Power Plant

Yidie Ye,[1] **Amil Daraz**,[1] **Abdul Basit**,[1] **Irfan Ahmed Khan**,[2] **and Salman A. AlQahtani**[3]

[1]*School of Information Science and Engineering, NingboTech University, Ningbo 315100, China*
[2]*Department of Electrical Engineering, Faculty of Engineering, Universiti Malaya, 50603 Kuala Lumpur, Malaysia*
[3]*Computer Engineering Department, College of Computer and Information Sciences, King Saud University, Riyadh, Saudi Arabia*

Correspondence should be addressed to Amil Daraz; amil.daraz@nbt.edu.cn

Received 9 January 2024; Revised 12 March 2024; Accepted 19 March 2024; Published 9 April 2024

Academic Editor: Yogendra Arya

To sustain a system frequency within acceptable limits, it is widely conceded that retaining a power balance between generation and demand is necessary. In order to regulate the frequency of power systems (PSs) this article proposes a novel cascaded based fractional-order controller termed as fractional-order integer- (FOI-) fractional-order proportional integral with double derivative (FOPIDD2). In addition to redox flow batteries and capacitive energy storage, the recommended control strategy has been validated with gas, thermal reheat, hydro, and nuclear power systems. Additionally, a newly designed algorithm known as squid game optimizer (SGO) optimizes the gains of the new FOI-FOPIDD2 controller. The squid game optimizer technique is inspired by the fundamental principles of a conventional Korean sport. It employs a population of candidate solutions and iteratively adjusts the control parameters to discover the optimal set that reduces frequency abnormalities and improves system stability. A comparison is also made between the controller's performance and benchmarks, including the jellyfish search algorithm, the firefly algorithm, the grey wolf optimizer, and the particle swarm algorithm. The proposed algorithms reduced peak overshoot as compared to grey wolf optimizer algorithm by 35.34%, 46.78%, and 76.89%; jellyfish search optimization algorithm by 34.76%, 77.22%, and 82.56%; and firefly algorithm by 82.67%, 89.23%, and 29.67% for frequency variations in area 1, area 2 and tie line power, respectively. Furthermore, SGO-FOI-FOPIDD2 controllers under different loading circumstances and conditions were evaluated and endorsed for their ability to withstand uncertainties in power system parameters.

1. Introduction

The modern interconnected power system (IPS) is designed with several control regions linked by tie lines. The daily energy demand is increasing as the world's population grows. Inconsistencies in load demand cause irregularities in both frequency and tie line power flow within the IPS's control zones. In order to overcome this challenge within the existing power system framework, load frequency regulators play an important role in balancing power consumption and generation [1, 2]. Both primary and secondary mechanisms play an important role in controlling frequency fluctuations. A governor uses a control method to alter the speed and frequency of basic control processes [3]. However, after considerable deviations, supplementary control is required to stabilize frequency. The secondary controller, therefore, is of greater importance to the overall performance of the system [4].

1.1. Literature Survey. The principal aim of load frequency control (LFC)/automatic generation control (AGC) is to regulate the power deviation between adjacent regions linked by tie lines within defined boundaries and maintain the system frequency within predetermined limits [5]. In the early stages of control scheme development for AGC, conventional controllers such as integral (I), proportional integral (PI), and PI derivative (D) were utilized. Researchers preferred these controllers due to their adaptability and simplicity; nevertheless, the outcomes frequently failed to meet expectations in terms of performance [6, 7]. For instance, in [8] proposed PID controller optimized with ant colony optimization (ACO) for single-area nuclear power system. The authors in reference [9] proposed PI controller to address the LFC problem in a single-area scenario incorporated with renewable energy resources. Researchers extended their investigations to tackle the LFC challenges arising in interconnected PSs. The researchers in [10] introduced an ACO algorithm for the purpose of optimizing the PID controller of a two-area interconnected nonreheat thermal power system with nonlinearity caused by governor dead band (GDB). Jagatheesan et al. in [11] proposed PI-based fuzzy logic controller for the frequency regulation of interconnected hydropower system incorporated with GDB as well as GRC nonlinearities. Apart from the conventional power systems, various researchers have worked in a deregulated power system by designing various types of controllers to regulate the frequency [12, 13].

Various control mechanisms have been introduced in PSs to address the issue of load frequency management. A few examples include model predictive control [14], robust sliding mode controllers [15], artificial intelligence-based LFC approach [16], linear matrix inequality [17], resilient control methodologies [18], data-driven controllers [19], fuzzy logic control (FLC) [20, 21], and robust virtual inertia control [22]. To control the frequency of connected PSs, the classic PID controller has been the principal focus of academic research because of its ease of use and low cost. Even yet, the PID controller has a difficult time adapting to nonlinear properties and interruptions in the system by trial and error. To determine the best PID values, a considerable amount of effort has been expended. Due to advances in computing power that enable simulation and accurate implementation of the fractional-order controller, the use of fractional-based controllers has recently drawn more attention in power engineering issues, specifically for power optimization control. The FOPID and their modification have been utilized in [23–25] as a secondary LFC to improve the frequency stability of the interconnected two region power systems. Numerous cascaded controller forms [26–28] have been used to improve frequency persistence in PSs. Recent research [29, 30] has investigated a second method for studying LFC that emphasizes the integration of two controllers. The frequency variations of a two-area coupled PS can be diminished using a PIDD2 controller framework, which was also proposed by authors in [31]. Moreover, references [32, 33] recommended the integral- (I-) tilt derivative (TD) and fractional-order (FO) I-TD controller for system frequency adaptation, respectively. The frequency effectiveness of the ID-T controller is superior to that of the TID controller [34].

There is numerous research in the literature that use fractional calculus to solve classical PID controller [35, 36]. According to previous research, FOPID and PIDD2 controllers can surpass PID controllers in numerous engineering applications in addition to the LFC system. To improve the control performance of LFC systems, an upgraded controller must be developed. As a result, for the first time, we proposed a cascaded based FOI-FOPIDD2 controller to enhance LFC transient and dynamic performance. The suggested controller can be viewed as a hybrid of fractional calculus and PIDD2.

Research has shown that selecting the controller type is just as important as choosing the controller settings. By utilizing evolutionary optimization to optimize controller parameters, the frequency stability problem has been greatly improved. New sophisticated methods are employed to adjust the controller coefficients to overcome the complexity of the control methods. For example, the researchers used the self-tuned algorithm (STA) [37], marine predator optimization algorithm (MPA) [38], chaos game optimization (CGO) [39], modified multiverse optimizer [40], improved based fitness-dependent optimizer [41], equilibrium optimizer hybridized with slime mould optimization algorithm [42], artificial ecosystem optimization (AEO) [43], sunflower optimization [44], butterfly optimization algorithm (BOA) [45], smell agent optimization (SAO) [46], pathfinder optimizer algorithm (PFA) [47], mine blast algorithm (MBA) [48], Fox optimizer algorithm (FOA) [49], and social-spider optimizer [50]. According to research [51], the TID with filter (TIDF) configured with DE outperformed the I/PI/PID controller. Similarly, in reference [52], the water cycle algorithm- (WCA-) tuned modified TID controller functioned more efficiently than PID/TID controllers.

This study is aimed at obtaining the right knobs for the recommended controller by developing a new metaheuristic algorithm called the squid game optimizer (SGO) technique, which is inspired by the fundamentals of a traditional Korean sport. During the squid game, attackers strive to reach their target, whereas players attempt to eradicate one another. It is typically acted on broad, open grounds with no predetermined extent and dimension limitations. Based on historical records, the playing area for this sport is commonly devised in a design resembling a squid and appears to be approximately half the dimensions of a standard basketball court. First, the numerical model of this approach is built by selecting the best nominee solutions and selecting an initialization method at random. In two groups, solution candidates move among defensive players, initiating a fight that is replicated by random movement towards defensive players. The position update procedure is completed, and the current position vectors are formed by judging the winner declarations of the players on opposite sides. These states are estimated based on the cost function. Twenty-five (25) unrestricted mathematical assessment functions are applied to examine the performance of the presented SGO algorithm, along with six others that regularly used metaheuristics for assessment

Table 1: List of nomenclature and notations.

Acronym	Definition
IPS	Interconnected power system
SGO	Squid game optimizer
AVR	Automatic voltage regulator
FA	Firefly algorithm
JSO	Jellyfish swarm optimization
SLP	Step load perturbation
PSO	Particle swarm optimization
ΔF	Frequency variation
PID	Proportional integral derivative
WCA	Water cycle algorithm
PIDD2	Proportional integral with double derivative
PIDF	Proportional-integral-derivative filter
ITAE	Integral time absolute error
CES	Capacitive energy storage
TIDN	Tilt integral derivative with filter
TF	Transfer function
FO	Fractional order
FLC	Fuzzy logic controller
PSO	Particle swarm optimization
TD	Time delay
RFB	Redox flow battery
T_{re}	Time constant for reheat turbine
K_{g}	Participation factor for gas
BDG	Biodiesel generator
K_{h}	Participation factor for hydro
CF	Cost function
β	Frequency bias factor
AGC	Automatic generation control
BES	Battery energy storage
ESS	Energy storage system
ITSE	Integral time square error
ΔPD	Load deviation
R	Speed regulation
ΔPG	Output deviation of a generator
FA	Firefly algorithm
Tp	Time constant of power system
O_{sh}	Overshoot
U_{sh}	Undershoot
Kp	Gain of power system
M	Inertia constant
ST	Settling time
JSO	Jellyfish search optimization
H	Power system gain
HMG	Hybrid microgrid
MG	Microgrid
U_{b}	Upper boundary
ΔXG	Valve position of governor

Table 1: Continued.

Acronym	Definition
ITSE	Integral time square error
L_{b}	Lower boundary
T_{w}	Wind time constant
T_{cr}	Combustion reaction time delay
X	Speed governor lead time constant
a, b, c	Constants of valve positioner
G_{N}	Participation factor for nuclear plant
K_{re}	Gain of reheat steam turbine
PS	Power system
Tw	Time constant for water
TCD	Compressor discharge volume time constant
a_{12}	Area size ratio
Y	Speed governor lag time constant
LFC	Load frequency control
BD	Boiler dynamics

[53]. Furthermore, the suggested SGO's capability is evaluated using advanced real-real-life challenges on the latest CEC, such as CEC 2020, with the SGO demonstrating remarkable results in haggling with these inspiring optimization challenges [53].

In addition, the primary conclusion drawn from the available literature is that LFC methods, such as FLC, H-infinite approaches, and model predictive control, which rely on the controller designer's imagination to achieve the desired performance, accomplish that despite numerous design flaws and a lengthy setup process. In addition, conventional PD/PI/PID controllers struggle with responding to uncertainty in the system. The impact of system nonlinearities and boundary fluctuations on robustness evaluations has been underexplored in several earlier works. Most previous evaluations also ignored the significant integration of energy storage devices (ESD) without adjusting system parameters due to the included system nonlinearities/uncertainties and immediate demand variations. The list of nomenclature and notations is shown in Table 1.

1.2. Contribution of the Paper. This research proposes a novel FOI-FOPIDD2 controller that improves system frequency steadiness as accounting for perturbations affected by diverse power sources. In accord with the SGO, the settings for the suggested FOI-FOPIDD2 controller have also been established to guarantee frequency and system constancy under atypical conditions. The main contribution of the paper is summarized as follows, in contrast to earlier studies on related subjects:

(i) Employing a reliable FOI-FOPIDD2 controller to enhance frequency reliability for dual zone coupled

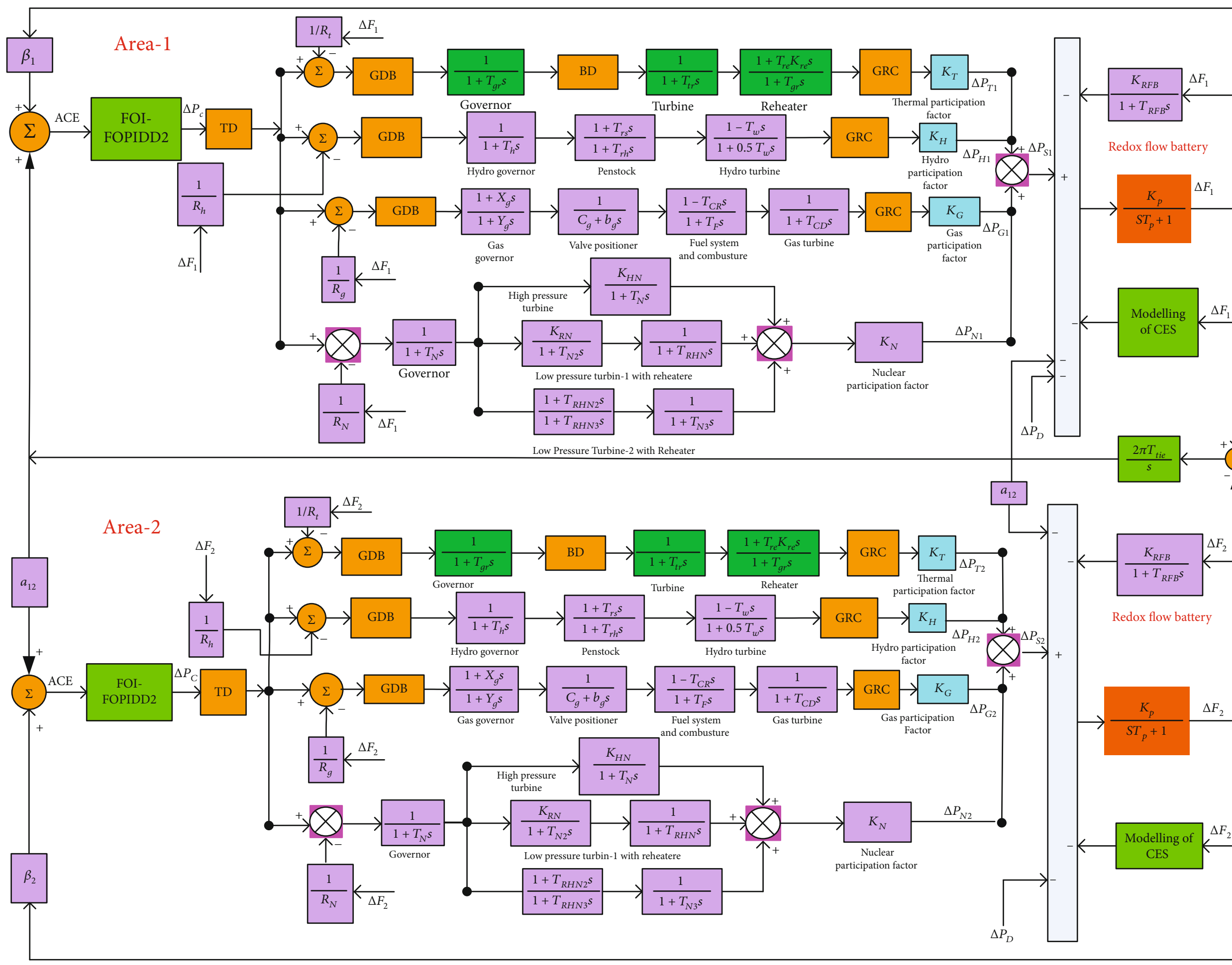

Figure 1: Dynamic modelling of the proposed PS.

power systems amalgamated with capacitor energy storage, hydro, nuclear, reheat thermal, gas, and redox flow battery

(ii) In order to refine the knobs of the presented FOI-FOPIDD2 controller, a novel strong algorithm termed as squid game optimizer (SGO) algorithm is presented for the diverse interconnected hybrid power systems

(iii) To validate the dominance of the proposed FOI-FOPIDD2 controller over the existing FOPID/PID/PIDD2 controller

(iv) The diverse hybrid power systems have been analyzed with the inclusion of various nonlinearities including time delay (TD), generation rate constraints (GRC), boiler dynamics (BD), and governor dead zone (GDB) to make the system realistic

(v) Exhibiting the supremacy of the SGO over other existing algorithms, such as the particle swarm optimization (PSO) algorithm, grey wolf optimizer (GWO), jellyfish swarm optimization (JSO), and firefly algorithm (FA)

(vi) Examine the robustness and stability of the proposed controller under extensive variation of the power system parameters and loads

2. Modelling of Hybrid Power System

In this portion, a dual area PS that is combined with reheat thermal, nuclear, gas, hydro, capacitor energy storage, and redox flow battery is mathematically modeled which is shown in Figure 1. The schematic diagram is shown in Figure 2. The distribution of all the included power generations between the two regions is assumed to be equal. The PS material from [24, 41, 54] is used to construct the system in Simulink/MATLAB and is available in Table 2. For the thermal system, the GRC of 10%/min is considered for both rising and dropping rates. Growing generation is utilized into consideration for the hydro portion at a typical GRC of 270%/min, while decreasing generation is considered into action at a regular GRC of

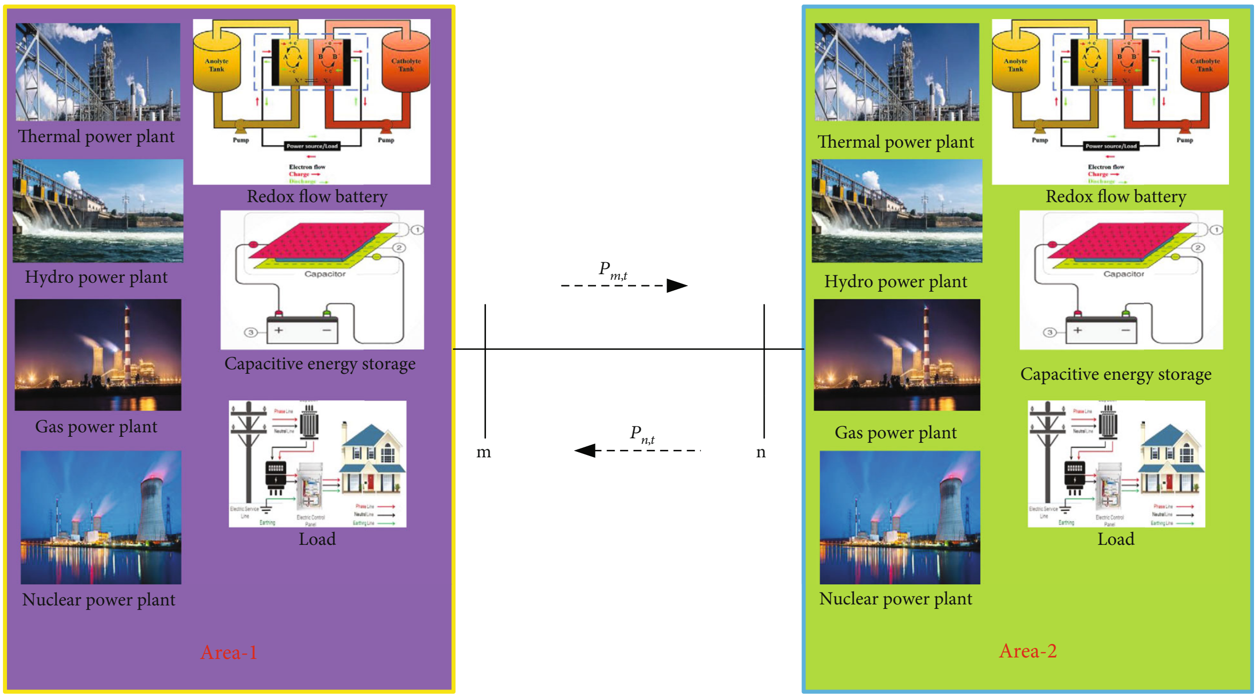

Figure 2: Schematic diagram of the proposed PS.

360%/min [12]. The mathematical formulation for GDB is described below [55].

$$\mathrm{GDB} = \frac{N_1 + sN_2}{sT_{\mathrm{sg}} + 1}, \tag{1}$$

where $N_1 = 0.8$ and

$$N_2 = \frac{-0.2}{\pi}. \tag{2}$$

Furthermore, a time delay (TD) of 2 seconds is inserted after the controller design to make the arrangement more realistic, which is given in equation (3). Similarly, a boiler dynamic is added as a nonlinearity into the thermal reheat system, and their schematic type is shown in Figure 3. The mathematical representation for the proposed boiler dynamics is also given in equation (4) [12, 55]. The area control error (ACE) for multigeneration unit is given in equation (5).

$$T_{\mathrm{f}}(s) = \frac{e^{-t_d(s)}}{sT + 1}, \tag{3}$$

$$T_{\mathrm{cpu}}(s) = \frac{K_{1\mathrm{b}}(I + sT_{1\mathrm{b}})(1 + sT_{\mathrm{rb}})}{(1 + 0.1T_{\mathrm{rb}}s)s}, \tag{4}$$

$$\mathrm{ACE} = \beta_i \Delta F_i + \Delta P\mathrm{tie}_{ij}, \quad i \neq j. \tag{5}$$

2.1. Modelling of Reheat Thermal, Hydro, Nuclear, and Gas Power Plants. Conventional power systems comprised of reheat thermal (with submodel of governor/turbine/reheater) and hydropower generation (with submodel of governor/penstock/droop compensation). The mathematical descriptions for reheating thermal structure with their subsequent submodel including (governor/turbine/reheater) are shown in the below equations, respectively [24, 28].

$$\begin{aligned}
G_{\mathrm{G}}(s) &= \frac{1}{sT_{\mathrm{gr}} + 1}, \\
G_{\mathrm{T}}(s) &= \frac{1}{sT_{\mathrm{tr}} + 1}, \\
G_{\mathrm{R}}(s) &= \frac{1 + T_{\mathrm{re}}K_{\mathrm{re}}s}{sT_{\mathrm{re}} + 1}, \\
G_{\mathrm{RT}}(s) &= \frac{1 + T_{\mathrm{re}}K_{\mathrm{re}}s}{(sT_{\mathrm{re}} + 1)(sT_{\mathrm{gr}} + 1)(sT_{\mathrm{tr}} + 1)}.
\end{aligned} \tag{6}$$

The mathematical representations for hydroelectric power with their subsequent submodel including governor/penstock/droop compensation are shown in the below equations, respectively [45, 55].

$$\begin{aligned}
G_{\mathrm{HG}}(s) &= \frac{1}{sT_{\mathrm{h}} + 1}, \\
G_{\mathrm{HT}}(s) &= \frac{1 + T_{\mathrm{rs}}s}{sT_{\mathrm{rh}} + 1}, \\
G_{\mathrm{HD}}(s) &= \frac{1 - T_{\mathrm{w}}s}{0.5T_{\mathrm{w}}s + 1}, \\
G_{\mathrm{H}}(s) &= \frac{(1 - T_{\mathrm{w}}s)(1 + T_{\mathrm{rs}}s)}{(sT_{\mathrm{h}} + 1)(1 + 0.5T_{\mathrm{w}}s)(sT_{\mathrm{rh}} + 1)}.
\end{aligned} \tag{7}$$

Table 2: [25, 41, 55, 57, 58].

LFC model			
T_{ps1}	11.49	K_{ps1}	68.97 Hz/p.u. MW
$R_{\mathrm{h}} = R_{\mathrm{t}} = R_{\mathrm{g}} = R_{\mathrm{N}}$	2.4 Hz/p.u. MW	K_{ps2}	68.97 Hz/p.u. MW
T_{ps2}	11.49	β_1	0.4312 Hz/p.u. MW
R_{T}	2.4	β_2	0.4312 Hz/p.u. MW
T_{tie}	0.0866 p.u. MW/rad		
Parameters and their values for hydropower system, reheat thermal, hydro nuclear, CES, and RFB			
T_{gr}	0.08 sec	T_{tr}	0.3 sec
T_{re}	10 sec	K_{re}	0.3
T_{h}	0.3 sec	T_{rs}	5 sec
T_{rh}	28.75 sec	T_{w}	0.0235 sec
K_{T}	0.5	T_{CR}	0.01 sec
C_{g}, c_{g2}	1	T_{F}	5
b_{g1}, b_{g2}	0.05	T_{CD}	0.2 sec
X_{g}	0.6	Y_{g}	1
T_{N}	0.05	K_{G}	0.25
K_{RN}	0.2	a_{12}	-1
T_{N2}	0.25	K_{H}	0.25
T_{RHN}	10 sec	T_{T}	0.3 sec
T_{RHN2}	10 sec	K_{RFB}	0.6
T_{RHN3}	0.25	K_{N}	0.25
T_{N3}	0.05 sec	T_{CES}	0.046 sec
K_{CES}	0.3	T_2	0.029 sec
T_1	0.280 sec	T_4	0.39 sec
T_3	0.0411 sec		
Boiler dynamic			
K_3	0.92	C_{b}	200
T_{f}	0.23	T_{rb}	0.545
T_{rh}	28.75	T_{r}	1.4
K_2	0.095	K_1	0.85
K_{1b}	0.950	T_{1b}	0.545

The nuclear power plant model consists of a governor, two low-pressure turbines (LPT), and a high-pressure turbine (HPT) shown in Figure 4. Equations (8)–(11) represent the transfer functions (TFs) of the governor, HPT turbine with reheater, LPT-1 with reheater, and LPT-2 with reheater, respectively [56, 57].

$$G_{\mathrm{N}}(s) = \frac{1}{sT_{\mathrm{N}} + 1}, \tag{8}$$

$$G_{\mathrm{HP}}(s) = \frac{K_{\mathrm{HN}}}{sT_{\mathrm{N1}} + 1}, \tag{9}$$

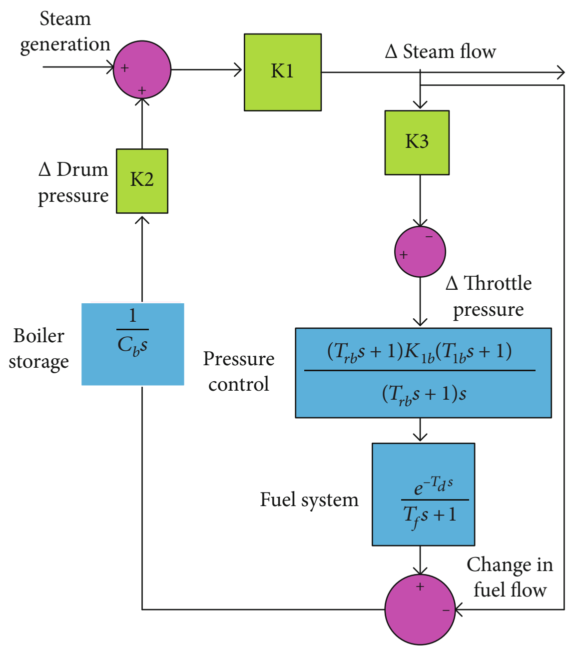

Figure 3: Schematic pattern of boiler dynamics.

$$G_{\mathrm{LP1}}(s) = \frac{K_{\mathrm{RN}}}{(sT_{\mathrm{N2}} + 1)(sT_{\mathrm{RHN1}} + 1)}, \tag{10}$$

$$G_{\mathrm{LP1}}(s) = \frac{(sT_{\mathrm{RHN2}} + 1)}{(sT_{\mathrm{N3}} + 1)(sT_{\mathrm{RHN3}} + 1)}. \tag{11}$$

The transfer functions (TFs) of the gas generation system, which includes the fuel system with combustor ($G_{\mathrm{GC}}(s)$), gas turbine ($G_{\mathrm{GT}}(s)$), (GFC), gas governor ($G_{\mathrm{GG}}(s)$), and valve positioner ($G_{\mathrm{GV}}(s)$) are expressed by [49, 57]

$$\begin{aligned} G_{\mathrm{GC}}(s) &= \frac{(1 - sT_{\mathrm{CR}})}{(sT_{\mathrm{F}} + 1)}, \\ G_{\mathrm{GT}}(s) &= \frac{1}{(sT_{\mathrm{CD}} + 1)}, \\ G_{\mathrm{GG}}(s) &= \frac{(1 + sX_{\mathrm{g}})}{(sY_{\mathrm{g}} + 1)}, \\ G_{\mathrm{GV}}(s) &= \frac{1}{(sb_{\mathrm{g}} + C_{\mathrm{g}})}. \end{aligned} \tag{12}$$

2.2. Capacitive Energy Storage (CES) Modeling. Due to its ability to rapidly charge and discharge with a substantial amount of power, capacitive energy storage devices are growing in favor of modern power systems [58]. The benefit of CES is that it responds to a boost in demand by producing an abundance of electricity. It is affordable and easy to use. It has a long service life and does not perform worse for it. A supercapacitor [59] serves as the CES system's main energy storage factor. Capacitor plates are utilized for retaining energy in the form of static charge. CES emits energy back into the grid when demand is at

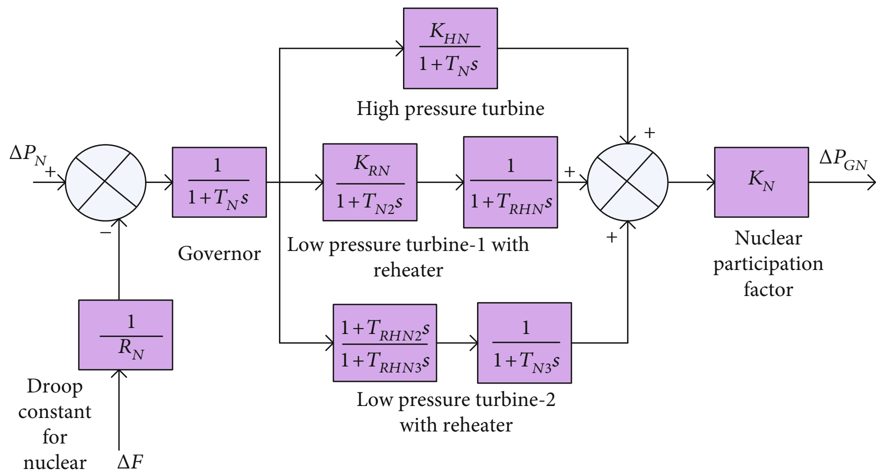

Figure 4: Transfer function model of nuclear power plant.

its highest. The modification in CES's incremental power is represented by [59]

$$\Delta P_{\text{CES}} = \left[\frac{K_{\text{CES}}}{(sT_{\text{CES}} + 1)}\right]\left[\frac{1 + sT_1}{(sT_2 + 1)}\right]\left[\frac{1 + sT_3}{(sT_4 + 1)}\right]\Delta F, \quad (13)$$

where $T_1 - T_4$ stand for the two-stage phase compensation blocks' time constants. Both analyzed PSs have incorporated CES scoring into their repertoires. The input control signal for each CES unit is the phase shift in frequency between two areas of the PS. The TF model of CES is shown in Figure 5.

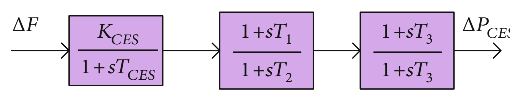

Figure 5: TF model of CES.

2.3. Modelling of Redox Flow Battery (RFB). RFB has become prevalent as a quick-rechargeable battery in recent times. An electrochemical transformation process is utilized in the redox progression, and a dual converter manages the rectifier and inverter functions. The benefit of the RFB is its rapid storage operation, which minimizes the impact on the environment by addressing the governor response delay and eliminating oscillations. RFB is made up of electrolyte, pumps, pipes, tanks, flow cells, and other modules that store energy during charging and release it under load demand [60, 61]. RFB can function at room temperature and is suitable for power ratings between kW and MW with storage durations of 2 to 10 hours [62]. Its control response time to frequency variations is particularly quick [63]. The key features that set RFB apart as an excellent ESD are its flexible power capability, low environmental effect, high efficiency, and versatility. Equation (14) shows the RBF transfer function [60, 61].

$$G_{\text{RFB}}(s) = \frac{K_{\text{RFB}}}{(sT_{\text{RFB}} + 1)}. \quad (14)$$

3. Squid Game Optimize

The proposed SGO algorithm is offered as a unique metaheuristic approach prompted by the basic rules of a traditional Korean sport. During the squid game, attackers strive to reach their target, whereas players attempt to eradicate one another. It is typically acted on broad, open grounds with no predetermined extent and dimension limitations. Based on historical records, the playing area for this sport is commonly devised in a design resembling a squid and appears to be approximately half the dimensions of a standard basketball court. First, the numerical model of this approach is built by selecting the best nominee solutions and selecting an initialization method at random. In two groups, solution candidates move among defensive players, initiating a fight that is replicated by random movement towards defensive players. The position update procedure is completed, and the current position vectors are formed by judging the winner declarations of the players on opposite sides. These states are estimated based on the cost function. Twenty-five (25) unrestricted mathematical assessment functions are applied to examine the performance of the presented SGO algorithm, along with six others that regularly used metaheuristics for assessment [53]. Furthermore, the suggested SGO's capability is evaluated using advanced real-real-life challenges on the latest CEC, such as CEC 2020, with the SGO demonstrating remarkable results in haggling with these inspiring optimization challenges [53]. SGO algorithms consist of the following steps [53].

3.1. Mathematical Formulation. In this section, the numerical description of the SGO method is considered employing the squid game strategy. The initialization technique is executed as follows in the initial step, with the search space treated as a specific area of the playing field and the prospective contenders (X_i) supposed to be players [53]:

$$X=\begin{bmatrix} X_1 \\ X_2 \\ \vdots \\ X_i \\ \vdots \\ X_n \end{bmatrix}=\begin{bmatrix} x_1^1 x_1^2 \cdots x_1^j \cdots x_1^d \\ x_2^1 x_2^2 \cdots x_2^j \cdots x_2^d \\ \cdots \ddots \vdots \\ x_i^1 x_i^2 \cdots x_i^j \cdots x_i^d \\ \cdots \ddots \vdots \\ x_n^1 x_n^2 \cdots x_n^j \cdots x_n^d \end{bmatrix}, \begin{cases} i=1,2,\cdots\cdots n, \\ j=1,2,\cdots\cdots d, \end{cases} \tag{15}$$

$$x_i^j = x_{i,\mathrm{Min}}^j + \mathrm{rand.}\left(x_{i,\mathrm{Max}}^j - x_{i,\mathrm{Min}}^j\right), \quad \begin{cases} i=1,2,\cdots\cdots n, \\ j=1,2,\cdots\cdots d. \end{cases} \tag{16}$$

Here, "n" signifies the overall count of players within the field, which corresponds to the search space. "d" denotes the dimensionality of the problem at hand. The initial position of the ith candidate is influenced by the j th decision variable, represented as x_i^j. The upper and lower bounds of the jth variable are termed as $x_{i,\mathrm{Max}}^j$ and $x_{i,\mathrm{Min}}^j$, respectively. The random number, denoted as "rand," follows a uniform distribution between 0 and 1. In the second phase of the algorithm, players are categorized into two equal-sized groups known as defensives (Def) and offensives (Off). Below is an algebraic depiction of these elements [53].

$$X^{\mathrm{off}}=\begin{bmatrix} X_1^{\mathrm{off}} \\ X_2^{\mathrm{off}} \\ \vdots \\ X_i^{\mathrm{off}} \\ \vdots \\ X_m^{\mathrm{off}} \end{bmatrix}=\begin{bmatrix} x_1^1 x_1^2 \cdots x_1^j \cdots x_1^d \\ x_2^1 x_2^2 \cdots x_2^j \cdots x_2^d \\ \cdots \ddots \vdots \\ x_i^1 x_i^2 \cdots x_i^j \cdots x_i^d \\ \cdots \ddots \vdots \\ x_m^1 x_m^2 \cdots x_m^j \cdots x_m^d \end{bmatrix}, \quad \begin{cases} i=1,2,\cdots\cdots m, \\ j=1,2,\cdots\cdots d, \end{cases}$$
$$X^{\mathrm{Def}}=\begin{bmatrix} X_1^{\mathrm{Def}} \\ X_2^{\mathrm{Def}} \\ \vdots \\ X_i^{\mathrm{Def}} \\ \vdots \\ X_m^{\mathrm{Def}} \end{bmatrix}=\begin{bmatrix} x_1^1 x_1^2 \cdots x_1^j \cdots x_1^d \\ x_2^1 x_2^2 \cdots x_2^j \cdots x_2^d \\ \cdots \ddots \vdots \\ x_i^1 x_i^2 \cdots x_i^j \cdots x_i^d \\ \cdots \ddots \vdots \\ x_m^1 x_m^2 \cdots x_m^j \cdots x_m^d \end{bmatrix}, \quad \begin{cases} i=1,2,\cdots\cdots m, \\ j=1,2,\cdots\cdots d. \end{cases} \tag{17}$$

Here, "m" represents the total count of players within each game group. The ith offensive player is denoted as X_i^{off}, and the kth defensive player is represented as X_i^{Def}. Once the game starts, an offensive player maneuvers among the defensive players to initiate a confrontation. It is important to highlight that each attacking player is constrained to move and engage in battle using a single foot, whereas defensive players have the liberty to use both feet. In mathematical terms, these elements are represented as follows [53]:

$$\mathrm{DG}=\frac{\sum_{i=1}^{m} X_i^{\mathrm{Def}}}{m}, \quad i=1,2,\ldots\cdots m,$$
$$X_i^{\mathrm{offNew1}}=\frac{X_i^{\mathrm{off}}+r_1\times \mathrm{DG}-r_2\times X_{r3}^{\mathrm{Def}}}{2}, \quad i=1,2,\ldots\cdots m. \tag{18}$$

Here, "r_1" and "r_2" denote two random numbers within the range of [0, 1], signifying the ability of the offensive players. "X_{r3}^{Def}" is a random integer ranging from 1 to "m". X_i^{offNew1} represents the position vector of the upcoming ith offensive player in the field, while "DG" stands for the defensive group. The subsequent step involves the evaluation of the objective function for each player, following a confrontation between the ith offensive player and a specific defensive player. The winning state (WS) of the players is then determined. If the offensive player emerges as the winner, based on the squid game's fundamental rules, they join the successful offensive group (SOG). The offensive player can use both feet for this purpose if the defensive player's winning state is lower than the offensive player's winning state. The mathematical representation of these aspects is articulated as [53]

$$X^{\mathrm{Sccoff}}=\begin{bmatrix} X_1^{\mathrm{Sccoff}} \\ X_2^{\mathrm{Sccoff}} \\ \vdots \\ X_i^{\mathrm{Sccoff}} \\ \vdots \\ X_o^{\mathrm{Sccoff}} \end{bmatrix}=\begin{bmatrix} x_1^1 x_1^2 \cdots x_1^j \cdots x_1^d \\ x_2^1 x_2^2 \cdots x_2^j \cdots x_2^d \\ \cdots \ddots \vdots \\ x_i^1 x_i^2 \cdots x_i^j \cdots x_i^d \\ \cdots \ddots \vdots \\ x_o^1 x_o^2 \cdots x_o^j \cdots x_o^d \end{bmatrix}, \quad \begin{cases} i=1,2,\cdots\cdots o, \\ j=1,2,\cdots\cdots d, \end{cases}$$
$$\mathrm{SOG}=\frac{\sum_{i=1}^{o} X_i^{\mathrm{Sccoff}}}{o}, \quad i=1,2,\ldots\cdots o,$$
$$X_i^{\mathrm{offNew2}}=X_i^{\mathrm{offNew1}}+r_1\times \mathrm{SOG}-r_2\times \mathrm{BSi}, \quad \mathrm{BSi}=1,2,\ldots\cdots m. \tag{19}$$

Defensive players are deemed the game's champions and are asked to join the SDG if their winning states are better than those of the offensive players. It is anticipated that the defensive players in this group will defend the bridge, the playground's pivotal feature. In preparation for starting a fresh fight, the thriving defensive players move among the attacking performers in the group. The mathematical appearance of these parts is given below [53].

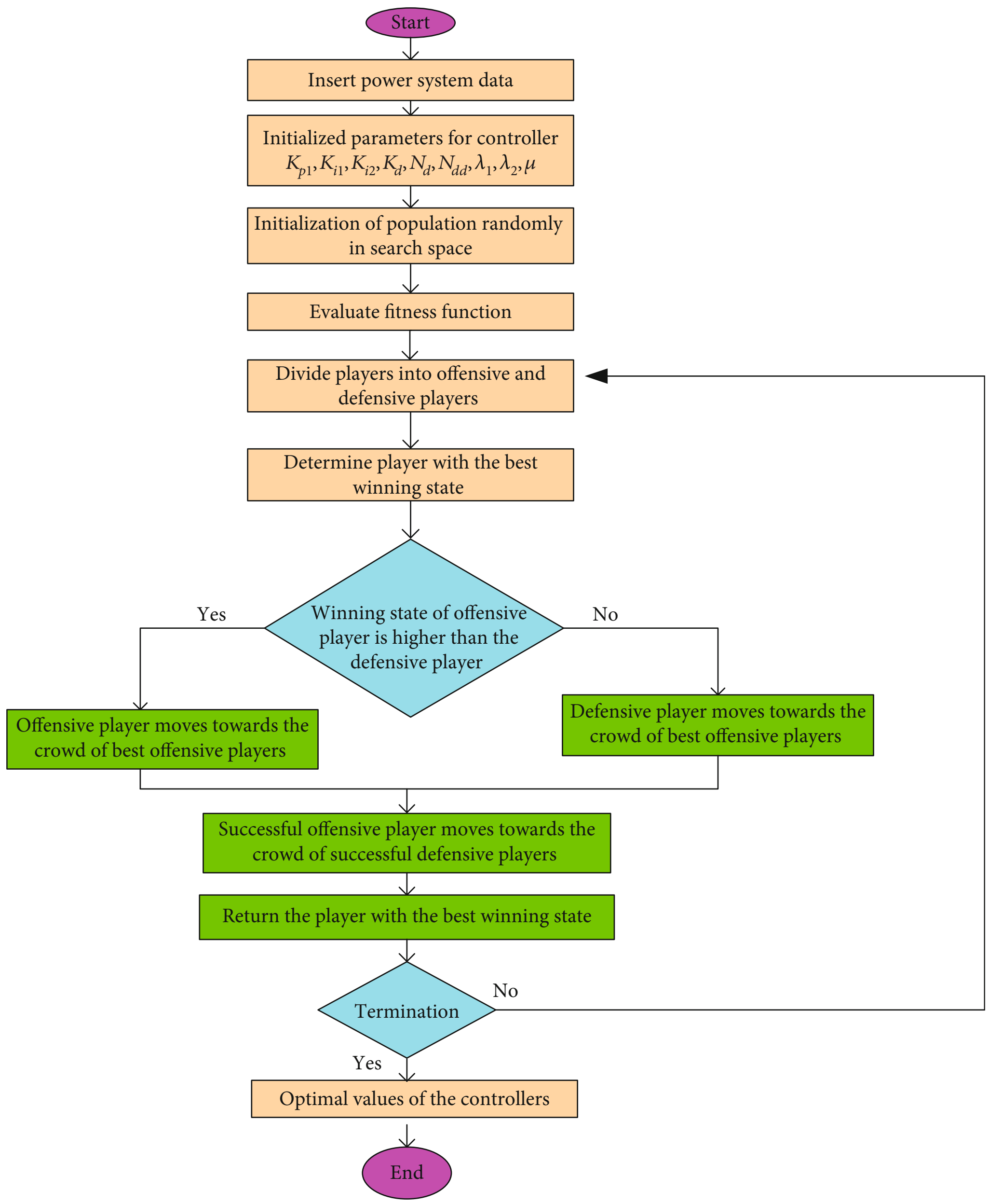

Figure 6: Flow diagram of SGO techniques.

$$\mathrm{SDG} = \begin{bmatrix} X_1^{\mathrm{Sccoff}} \\ X_2^{\mathrm{Sccoff}} \\ \vdots \\ X_i^{\mathrm{Sccoff}} \\ \vdots \\ X_p^{\mathrm{Sccoff}} \end{bmatrix} = \begin{bmatrix} x_1^1 x_1^2 \cdot \cdots x_1^j \cdot \cdots x_1^d \\ x_2^1 x_2^2 \cdot \cdots x_2^j \cdot \cdots x_2^d \\ \cdots \quad \ddots \quad \vdots \\ x_i^1 x_i^2 \cdot \cdots x_i^j \cdot \cdots x_i^d \\ \cdots \quad \ddots \quad \vdots \\ x_p^1 x_p^2 \cdot \cdots x_p^j \cdot \cdots x_p^d \end{bmatrix}, \quad \begin{cases} i = 1, 2, \cdot \cdots \cdots p, \\ j = 1, 2, \cdot \cdots \cdots d, \end{cases}$$

$$\mathrm{OG} = \frac{\sum_{i=1}^{m} X_i^{\mathrm{off}}}{m}, \quad i = 1, 2, .. \cdots m,$$

$$X_i^{\mathrm{DefNew1}} = \frac{X_i^{\mathrm{Def}} + r_1 \times \mathrm{OG} - r_2 \times X_{r3}^{\mathrm{off}}}{2}, \quad i = 1, 2, .. \cdots m. \tag{20}$$

The algorithm introduces an additional search loop, where offensive players within the successful offensive group (SOG) endeavor to navigate a bridge guarded by defensive players in the successful defensive group (SDG). This inclusion is aimed at intelligently adapting the exploration and exploitation phases of the proposed algorithm. To achieve this, a position-updating operation is executed for all offensive players in SOG, involving advancement towards the best-known solution candidate and a specific defensive player in SDG. This simulates the reward for an offensive player attempting to cross the bridge. The mathematical expression of these components is detailed as follows [53]:

$$X_i^{\mathrm{offNew1}} = \frac{X_i^{\mathrm{Scoff}} + r_1 \times \mathrm{BS} - r_2 \times X_k^{\mathrm{ScDef}}}{2}, \quad \begin{cases} i = 1, 2, .. \cdots o, \\ k = 1, 2, .. \cdots p. \end{cases} \tag{21}$$

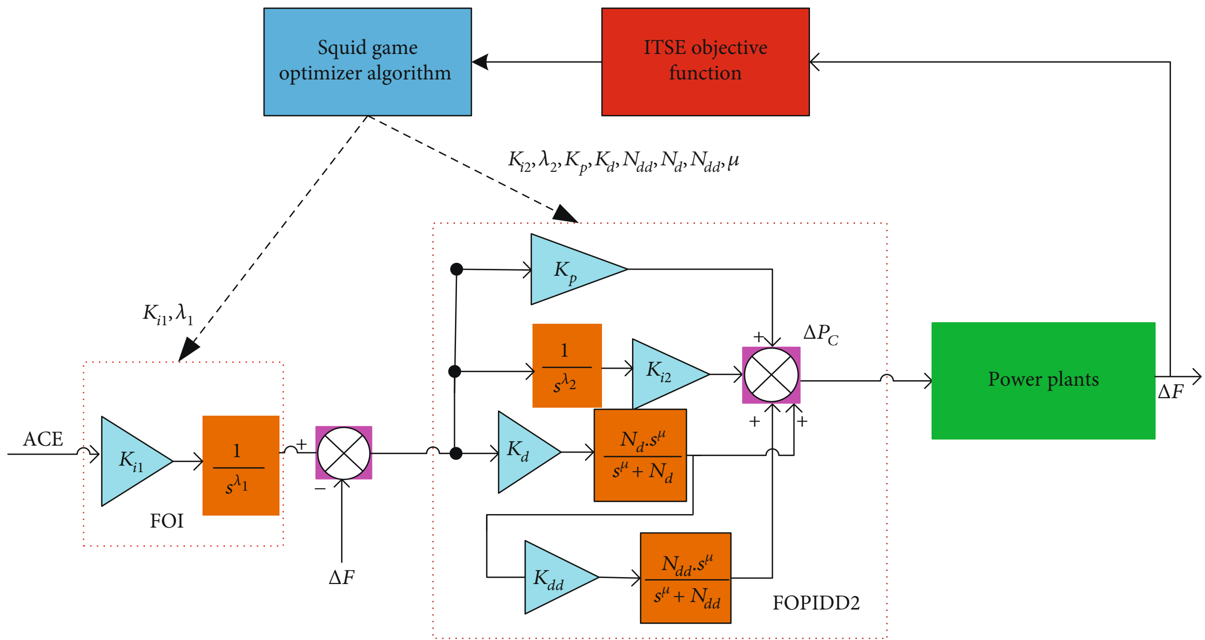

Figure 7: Structure of suggested FOI-FOPIDD2.

In SOG and SDG, p and o are the number of effective defensive and offensive players and "BS" represents the best solution candidate. The flow diagram for the proposed SGO method is depicted in Figure 6.

4. Design of Cascaded Based Controllers and Expression of Fitness Function

4.1. Concept of Fractional Order. Fractional calculus is a field of mathematical analysis that expands traditional calculus to include integrators and differentiators with noninteger orders. These orders are represented as $_aD_t^\gamma$, where "a" and "t" indicate the operation boundaries and γ is a real number (R). The formulas for fractional-order integrator and differentiator can be expressed as follows [64, 65]:

$$ {}_aD_t^\gamma = \begin{cases} \dfrac{d^\gamma}{dt^\gamma}, & \gamma > 0, \\ 1, & \gamma = 0, \\ \displaystyle\int_a^t (d\tau)^\gamma, & \gamma < 0. \end{cases} \tag{22}$$

The field of fractional calculus is guided by three essential principles: the Riemann-Liouville (RL) principle, the Caputo principle, and the Grunwald-Letnikov (GL) principle. These principles are represented by equations (14)–(16) correspondingly [64, 65].

$$\begin{aligned} {}_aD_t^\gamma f(f) &= \frac{1}{\Gamma(n-r)} \frac{d^n}{dt^n} \int_a^t \frac{f(\tau)d(\tau)}{(t-\tau)^{\gamma-n+1}} ; n-1<\gamma<n, \\ {}_aD_t^\gamma f(f) &= \frac{1}{\Gamma(n-r)} \int_a^t \frac{f^n(\tau)d(\tau)}{(t-\tau)^{\gamma-n+1}} ; n-1<\gamma<n, \\ {}_aD^a t^\gamma f(t) &= \lim_{b\longrightarrow 0} \frac{1}{b^\gamma} \sum_{j=0}^{[(t-a)/b]} (-1)^j \binom{\gamma}{j} f(t-jb). \end{aligned} \tag{23}$$

Mathematically, the αth fractional-order (FO) derivative, denoted as S^α, can be represented as follows [25]:

$$S^\alpha = \omega_h^\alpha \prod_{K=-N}^{N} \frac{s+\omega_k^z}{s+\omega_k^p}. \tag{24}$$

In this study, oustaloup-based recursive approximations are applied with a filter order of 5 and within the range of $[10^{-3}, 10^3]$ rad/s. The primary objective of the new design of the cascaded controller is to regulate and enhance the frequency response of a diverse power system coping with immediate load variations and variations. The controller has been recommended in both regions to reduce fluctuations in frequency and interconnected tie line power discrepancies between both regions. Conventional PID controllers are commonly utilized in manufacturing due to their straightforward design and efficient functioning. Like the standard PID structure, the PIDD2 assembly also incorporates a second-order derivative gain [66]. The FOI-FOPIDD2 controller has not yet been utilized in a study, despite numerous approaches being tested to improve the control performance of LFC systems. Researchers have shown that PIDD2 and FOPIDD controllers outperform traditional PID controllers. Figure 7 displays the cascaded based FOI-FOPIDD2 controller that was established by fusing FOPIDD2 controller and fractional-order integral controller.

Equations (25) and (26) describe the transfer function of the FOI and FOPIDD2 controllers. Similarly, equation (27) illustrates the connection between the system's output and the error signal.

$$\mathrm{FOI} = C_1(s) = \frac{K_{i1}}{s^{\lambda 1}}, \tag{25}$$

Table 3: Optimal values for the recommended methods.

	Approach	Kp	K_i	K_{i1}	K_{i2}	K_d	K_{dd}	N_d	N_{dd}	μ	λ_1	λ_2
Area 1	SGO: FOI-FOPIDD2	3.875	—	4.566	3.565	3.980	5.322	7.234	5.405	0.122	0.054	0.032
	JSO: FOI-FOPIDD2	1.090	—	3.783	2.989	1.678	7.778	9.772	7.012	0.378	0.252	0.098
	PSO: FOI-FOPIDD2	1.120	—	2.109	3.120	1.989	3.345	3.300	4.890	0.045	0.458	0.212
	GWO: FOI-FOPIDD2	3.456	—	1.900	1.123	1.110	2.657	6.090	5.780	0.157	0.234	0.114
	FA: FOI-FOPIDD2	5.101	—	2.546	2.787	2.079	8.456	8.567	4.781	0.056	0.767	0.098
	FOI-FOPIDD2: SGO	4.101	—	1.989	3.897	4.671	5.322	9.566	8.456	0.452	0.286	0.097
	FOPID: SGO	1.234	0.53	—	—	3.980	—	—	—	0.042	0.223	—
	PIDD2: SGO	4.760	3.45	—	—	2.974	6.897	4.678	9.898	—	—	—
	PID: SGO	3.12	2.89	—	—	7.789	—	—	—	—	—	—
Area 2	SGO: FOI-FOPIDD2	8.908	—	0.345	1.232	5.780	9.678	1.090	7.898	1.223	1.009	0.011
	JSO: FOI-FOPIDD2	5.776	—	7.879	3.345	4.445	3.390	9.878	4.454	1.909	2.000	1.019
	PSO: FOI-FOPIDD2	8.902	—	3.452	5.776	3.389	5.990	9.999	3.334	0.345	1.209	0.345
	GWO: FOI-FOPIDD2	5.346	—	3.786	7.090	3.786	1.298	7.897	1.909	1.123	0.009	0.465
	FA: FOI-FOPIDD2	5.090	—	2.786	4.570	8.019	3.678	3.435	5.009	1.543	0..675	1.010
	FOI-FOPIDD2: SGO	8.111	—	4.567	9.890	2.991	5.900	2.567	9.090	1.902	1.223	1.070
	FOPID: SGO	2.134	4.67	—	—	1.980	—	—	—	1.090	0.903	—
	PIDD2: SGO	1.340	9.34	—	—	5.909	9.009	1.903	8.000	—	—	—
	PID: SGO	4.12	9.87	—	—	2.009	—	—	—	—	—	—

Table 4: Value of SGO parameters.

Parameters	Values	Parameters	Values	Parameters	Values	Parameters	Values
Population number	30	No. of iteration	80	Lower limit	-10	Upper limit	10
No. of dimension	10	Random numbers	[0, 1]	Execution of each iteration	25		

Table 5: Statistical parametric analysis for various techniques.

Techniques	Statistical parameters			
	Best	Worst	Mean	Standard deviation
SGO: FOI-FOPIDD2	4.57×10^{-5}	4.58×10^{-5}	4.58×10^{-5}	4.57×10^{-7}
JSO: FOI-FOPIDD2	7.23×10^{-4}	7.28×10^{-4}	7.25×10^{-4}	0.96×10^{-6}
GWO: FOI-FOPIDD2	8.01×10^{-4}	8.11×10^{-4}	8.08×10^{-4}	9.23×10^{-6}
FA: FOI-FOPIDD2	3.45×10^{-3}	3.52×10^{-3}	3.49×10^{-3}	2.43×10^{-5}
PSO: FOI-FOPIDD2	3.02×10^{-3}	3.34×10^{-3}	3.28×10^{-3}	6.89×10^{-5}

$$\begin{aligned} \mathrm{FOPIDD2} = C_2(s) &= \mathrm{Kp} + \frac{K_{i2}}{s^{\lambda 2}} + K_d\left[\frac{N_d s^{\mu}}{s^{\mu} + N_d}\right] \\ &\quad + K_d\left[\frac{N_d s^{\mu}}{s^{\mu} + N_d}\right].K_{dd}\left[\frac{N_{dd} s^{\mu}}{s^{\mu} + N_{dd}}\right], \end{aligned} \tag{26}$$

$$\begin{aligned} U(s) = \Bigg[\mathrm{Kp} &+ \frac{K_{i1}}{s^{\lambda 1}} + \frac{K_{i2}}{s^{\lambda 2}} + K_d\left[\frac{N_d s^{\mu}}{s^{\mu} + N_d}\right] \\ &+ K_d\left[\frac{N_d s^{\mu}}{s^{\mu} + N_d}\right].K_{dd}\left[\frac{N_{dd} s^{\mu}}{s^{\mu} + N_{dd}}\right]E(s), \end{aligned} \tag{27}$$

where λ_1, λ_2, and μ are the integral-differentiator operators; N_d and N_{dd} denote the filter constants; and Kp, K_d, K_{i1}, and K_{i2} indicate the proportional, derivative, and integral coefficients of the proposed controller. The FOI-FOPIDD2 controller gains have been established by reducing the cost function through the utilization of the SGO. The settling period is shortened, and high oscillations are swiftly suppressed using an ITSE-based cost function [25, 33, 37]:

$$\mathrm{ITSE} = j = \int_o^t t\left[\Delta F_1^2 + \Delta F_2^2 + \Delta P_{\mathrm{tie}}^2\right]dt. \tag{28}$$

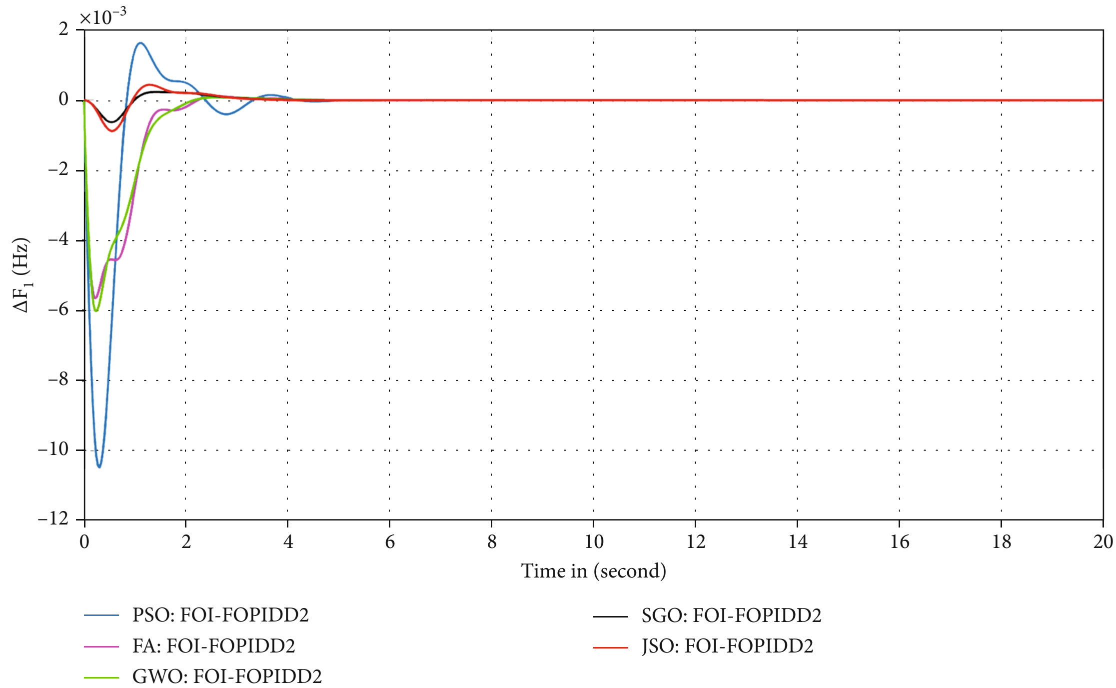

(a)

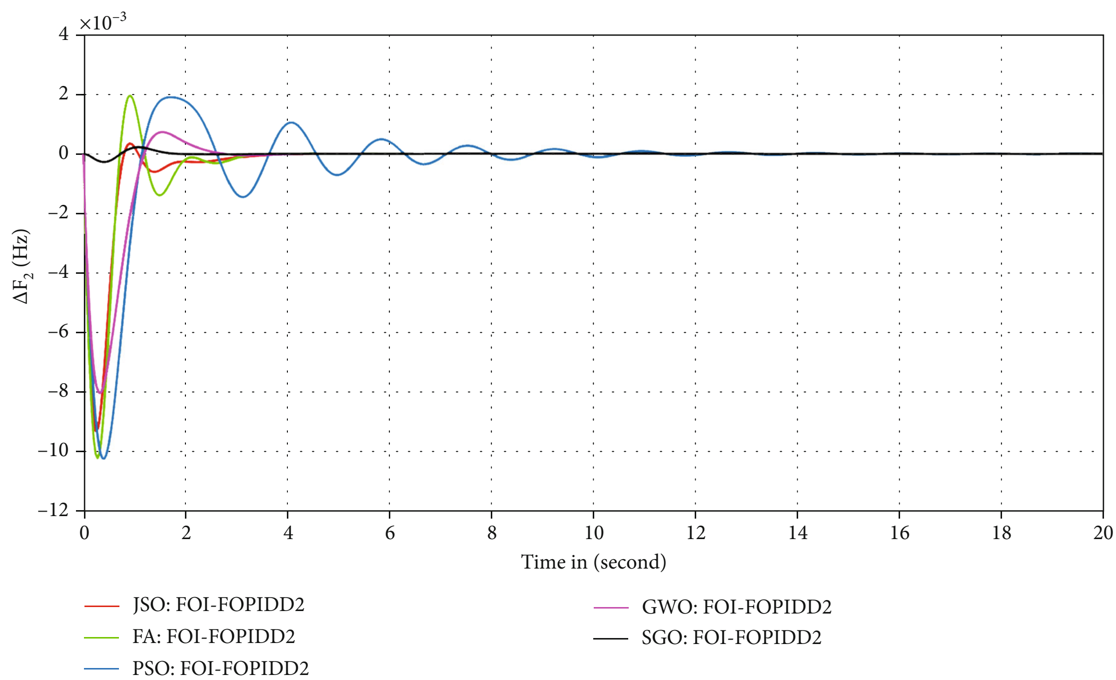

(b)

FIGURE 8: Continued.

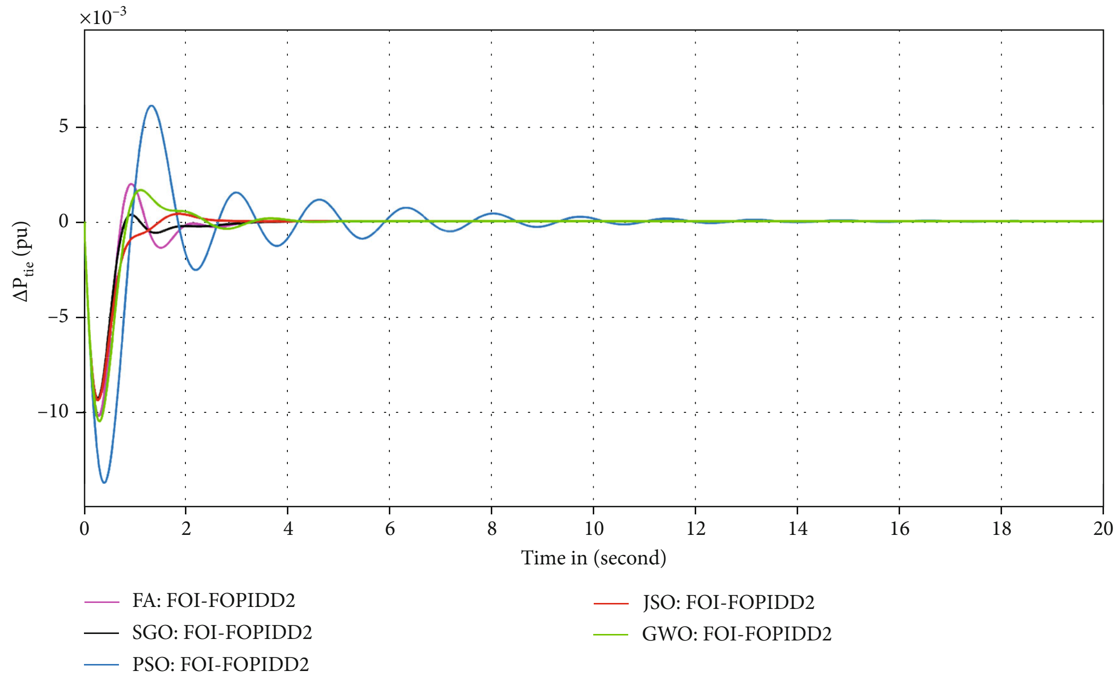

(c)

Figure 8: Transient response of PS considering case 1 for (a) ΔF_1, (b) ΔF_2, and (c) ΔP_{tie}.

Table 6: Comparison performance for case 1.

Transient parameters	Variation in areas	PSO	FA	GWO	JSO	SGO	WCA [52]
Time settling	ΔF_1	4.01	3.29	2.83	2.34	2.22	12.27
	ΔF_2	11.93	3.23	2.64	2.90	1.52	29.46
	ΔP_{tie}	12.11	3.66	3.83	3.07	2.81	30.50
Overshoot	ΔF_1	0.001632	0.000076	0.000123	0.0004376	0.0002347	0.00280
	ΔF_2	0.001890	0.001949	0.000725	0.0003407	0.0002201	0.00110
	ΔP_{tie}	0.006044	0.001949	0.001710	0.0003834	0.0003508	0.0007
Undershoot	ΔF_1	-0.010480	-0.00601	-0.00654	-0.0008692	-0.000615	-0.0109
	ΔF_2	-0.010240	-0.01022	-0.00803	-0.0093020	-0.000268	-0.0035
	ΔP_{tie}	-0.013700	-0.01022	-0.01049	-0.009516	-0.009405	-0.0022

Table 7: Comparison performance for case 2.

Transient parameters	Variation in areas	PID	PIDD2	FOPID	FOI-FOPIDD2	FOPI-PD [25]	FOTID [47]	I-TD [52]
Time settling (Ts)	ΔF_1	3.80	3.66	2.86	2.69	8.434	25.5	12.27
	ΔF_2	4.85	4.09	3.93	3.21	10.90	23.2	29.46
	ΔP_{tie}	3.83	3.71	3.66	3.20	5.98	18.77	30.50
Overshoot (O_{sh})	ΔF_1	0.00194	0.00007	0.00043	0.00024	0.00004	0.00680	0.00280
	ΔF_2	0.00044	0.00024	0.00028	0.00023	0.00027	0.01170	0.00110
	ΔP_{tie}	0.00241	0.00072	0.00012	0.00007	0.00000	0.00260	0.0007
Undershoot (U_{sh})	ΔF_1	-0.0102	-0.00600	-0.00086	-0.00061	-0.00059	-0.0245	-0.0109
	ΔF_2	-0.0008	-0.00062	-0.00035	-0.00026	-0.00178	-0.0228	-0.0035
	ΔP_{tie}	-0.0087	-0.00803	-0.00564	-0.00601	-0.00084	-0.0044	-0.0022

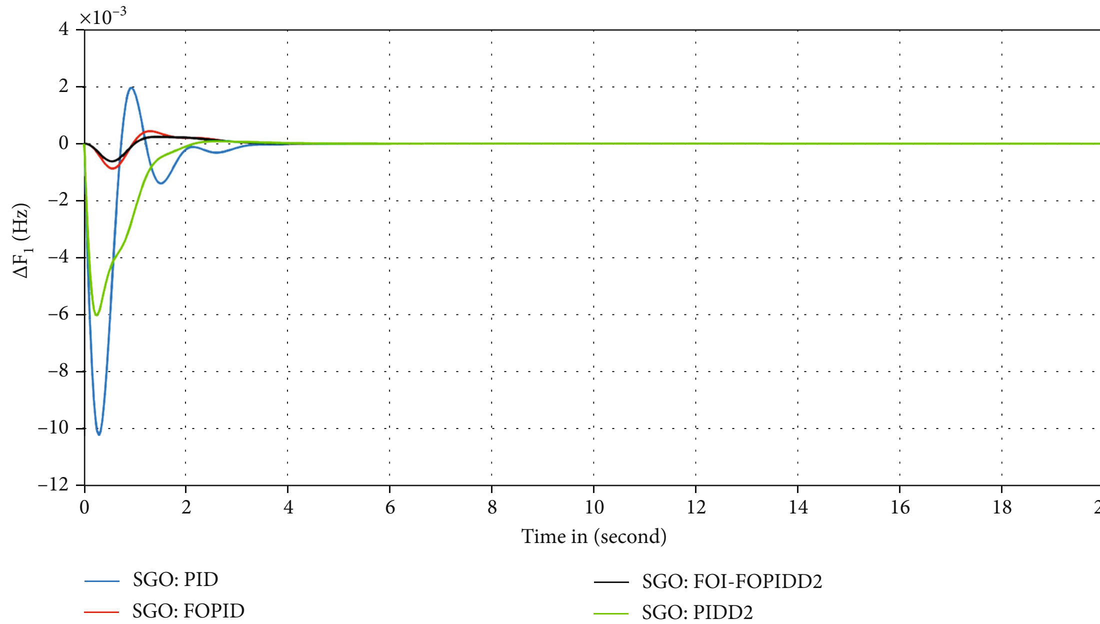

(a)

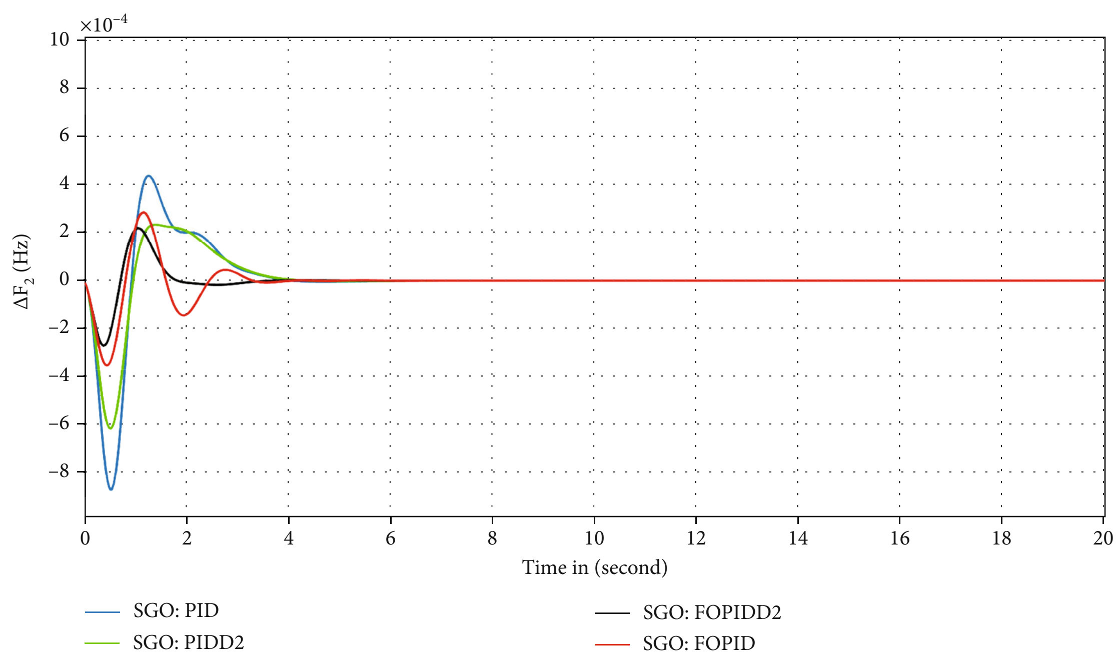

(b)

FIGURE 9: Continued.

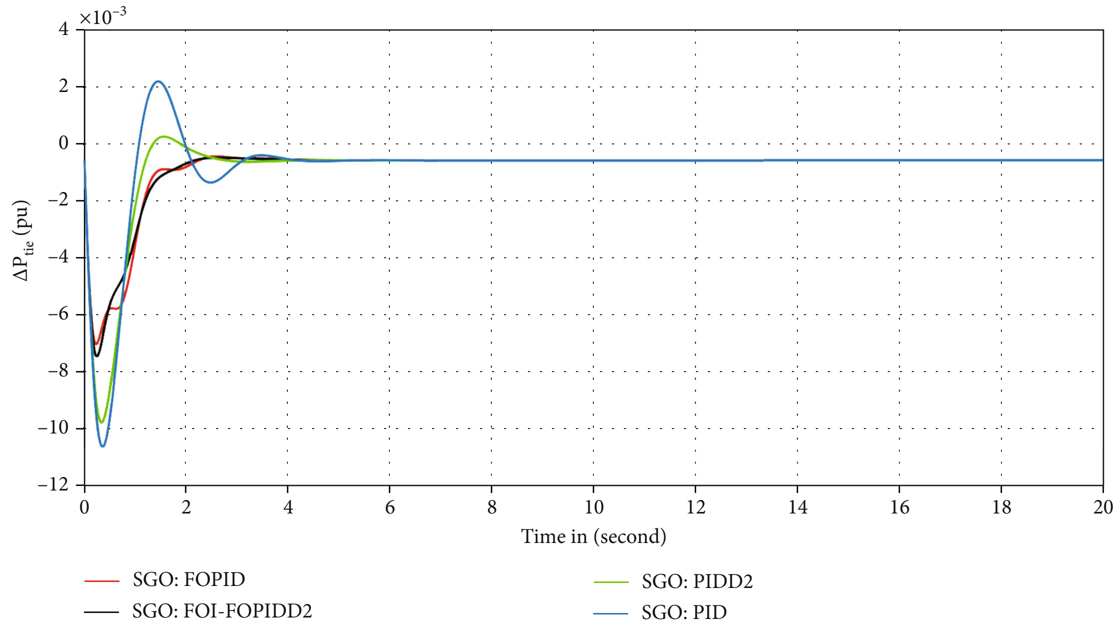

(c)

Figure 9: Transient response of PS considering case 2 for (a) ΔF_1, (b) ΔF_2, and (c) ΔP_{tie}.

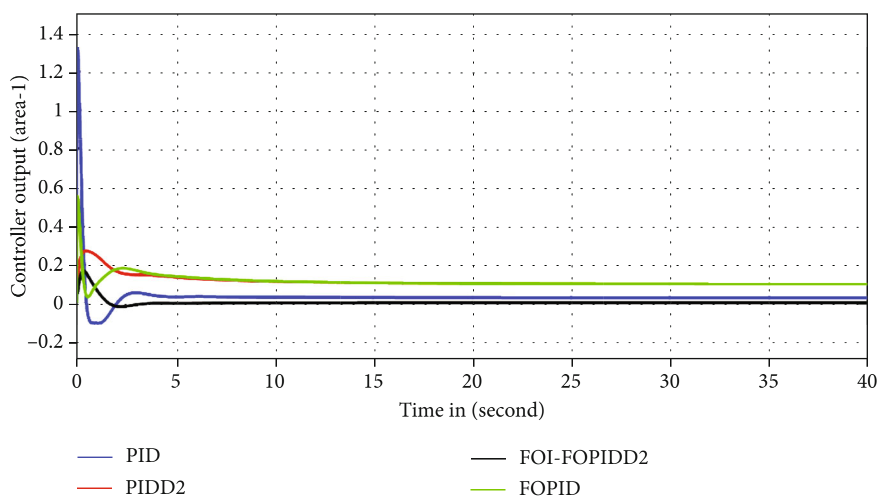

Figure 10: Controller efforts for various controllers in area 1.

The FOI-FOPIDD2 controller gains are subject to the following restrictions.

$$\begin{aligned} K_p^{\text{Min}} &\le K_p \le K_p^{\text{Max}}; K_d^{\text{Min}} \le K_d \le K_d^{\text{Max}}; K_{dd}^{\text{Min}} \le K_{dd} \\ &\le K_{dd}^{\text{Max}}; K_{i1}^{\text{Min}} \le K_{i1} \le K_{i1}^{\text{Max}}; K_{i2}^{\text{Min}} \le K_{i2} \\ &\le K_{i2}^{\text{Max}}; N_{dd}^{\text{Min}} \le N_{dd} \le N_{dd}^{\text{Max}}, N_d^{\text{Min}} \le N_d \\ &\le N_d^{\text{Max}}; {\lambda_1}^{\text{Min}} \le \lambda_1 \le {\lambda_1}^{\text{Max}}; {\lambda_2}^{\text{Min}} \le \lambda_2 \\ &\le {\lambda_2}^{\text{Max}}; N_d^{\text{Min}} \le N_d \le N_d^{\text{Max}}; \mu^{\text{Min}} \le \mu \le \mu^{\text{Max}}. \end{aligned} \tag{29}$$

The range of values for the parameters Kp, K_{i1}, K_{i2}, K_d, N_d, and N_{dd} is from 0 to 10, while the values for λ_1, λ_2, and μ are from 0 to 2.

5. Results, Execution, and Discussion

This study uses a combination of several hybrid power sources coupled with redox flow battery (RBF) and capacitor energy storage to test the effectiveness and validity of a novel FOI-FOPIDD2 controller. To meet the LFC goal function, the proposed controller coefficients are tweaked with the squid game optimizer utilizing the MATLAB programming language and connected with the Simulink tool. The SGO-based controller knobs for the specified case study are indicated in Table 3 following 80 iterations of the optimization techniques using the materials from Table 4. The statistical values foe various techniques are shown in Table 5. While employing the same alignment with the RFB system that uses the SGO technique, the suggested FOI-FOPIDD2

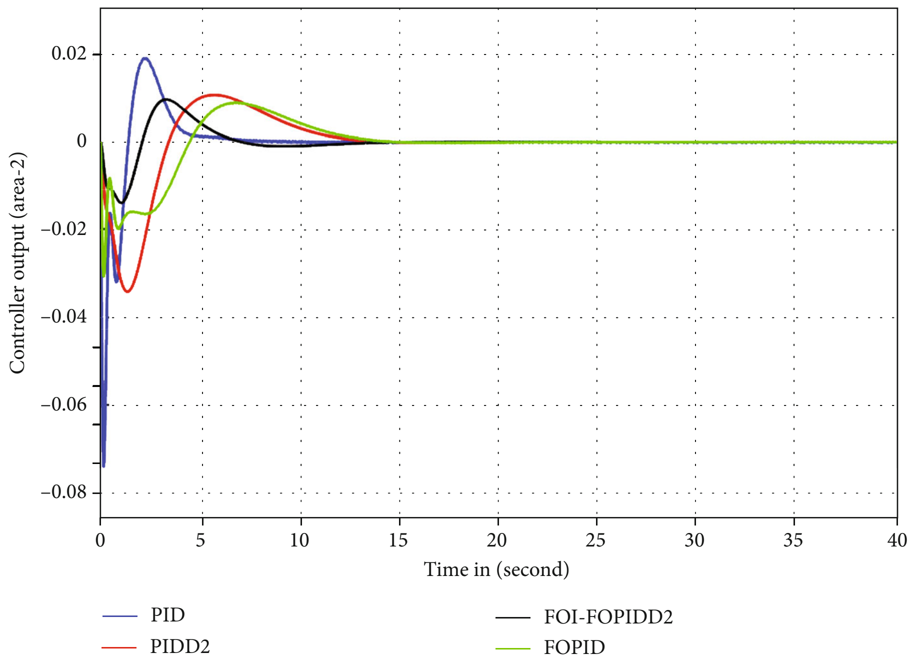

Figure 11: Controller efforts for FOI-FOPIDD2 in area 2.

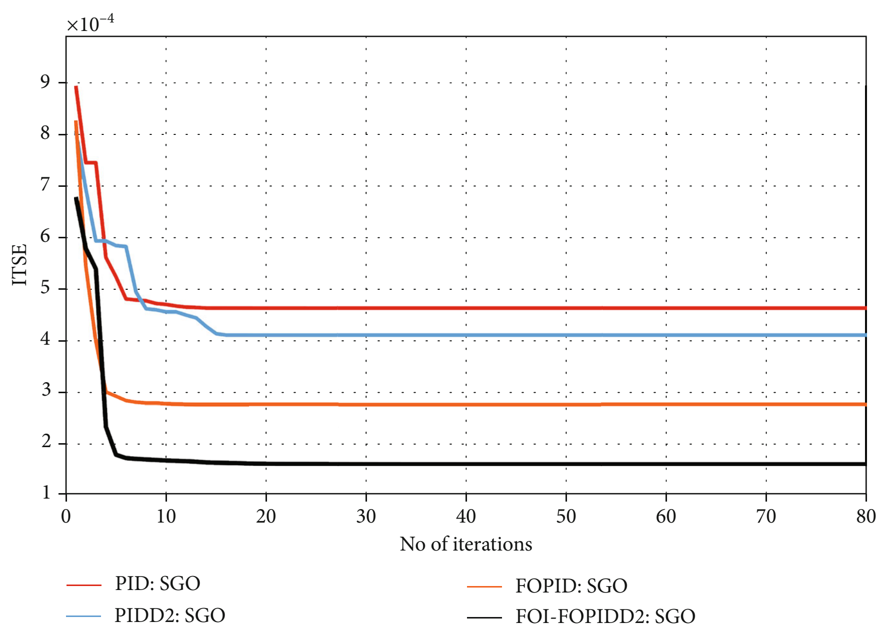

Figure 12: Convergence diagram for various controllers.

controller's robustness is compared to other regulators like PIDD2, PID, and FOPID. The load changes are fixed at 5% = 0.05 per unit, in all cases. Results from the examined multiarea IPS are rigorously examined in the subsequent case studies.

5.1. Case 1 (Analyses of Algorithm Performance). The squid game algorithm was compared with various recent algorithms including JSO, PSO, GWO, and firefly algorithm to determine its efficacy in this scenario. Each algorithm response was measured in terms of area 2 (ΔF_2), tie line (ΔP_{tie}), and area 1 (ΔF_1) as shown in Figures 8(a)–8(c). In Table 6, the overall performance is contrasted for various approaches in respect of transient parameters like U_{sh} (undershoot), O_{sh} (overshoot), and Ts (settling time) for ΔP_{tie}, ΔF_2, and ΔF_1. The SGO strategy offered quicker settling times than JSO, GWO, PSO, and FA-based optimization approaches in regions 1 and 2 and the linked tie line. The

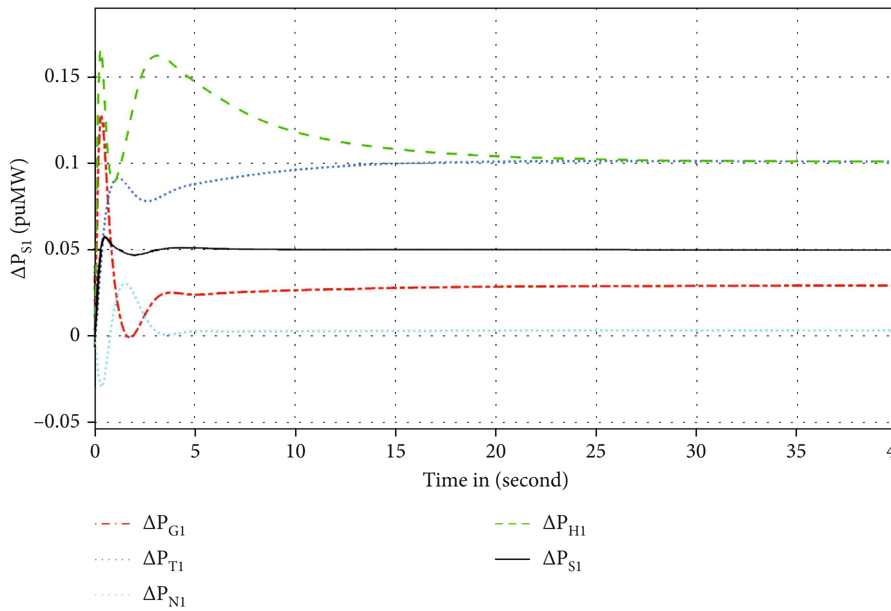

FIGURE 13: Power output for various generation units in area 1.

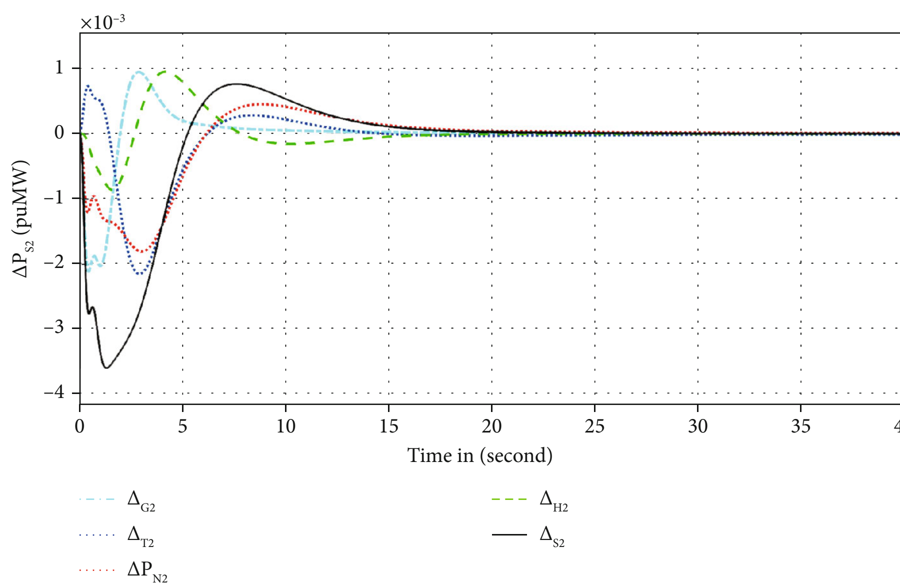

FIGURE 14: Power output for various generation units in area 2.

SGO approach decreased overshoot for ΔF_1, ΔF_2, and ΔP_{tie} by 81.23%, 45.76%, and 35.22%, respectively, as compared to PSO algorithm. Additionally, our intended method improved the settling time by 14.54%, 20.12%, and 15.34% as compared to PSO algorithms. The SGO algorithms also improve Ts by 22.34%, 09.87%, and 34.89% when compared to GWO algorithm, while also significantly lowering maximum O_{sh} by 71.12%, 72.99%, and 84.17% and undershoot by 80.09%, 36.87%, and 87.76% for ΔF_1, ΔF_2, and ΔP_{tie}. When comparing the GSO algorithm with the FA optimizer algorithm, improvements of 12.23% for ΔP_{tie}, 31.98% for ΔF_2, and 29.76% for ΔF_1 are observed in terms of Ts.

5.2. Case 2 (Analyses of Controller's Performance). This study compared the performance of the FOI-FOPIDD2 controller to that of other control approaches, such as FOPID, PIDD2, PID, and FOTID [47], I-TD [52], and FOPI-PDF [25], in terms of overshoot (O_{sh}), minimum undershoot (U_{sh}), and time settling (Ts), taking into account changes in area 2 (ΔF_2), tie line (ΔP_{tie}), and area 1 (ΔF_2). Overall, Table 7 compares the performance of each optimization procedure using transient metrics. Based on the data shown in Figures 9(a)–9(c) and Table 7, it appears that the FOI-FOPIDD2 control approach performed better than the other control techniques. When compared to the FOPID, PIDD2,

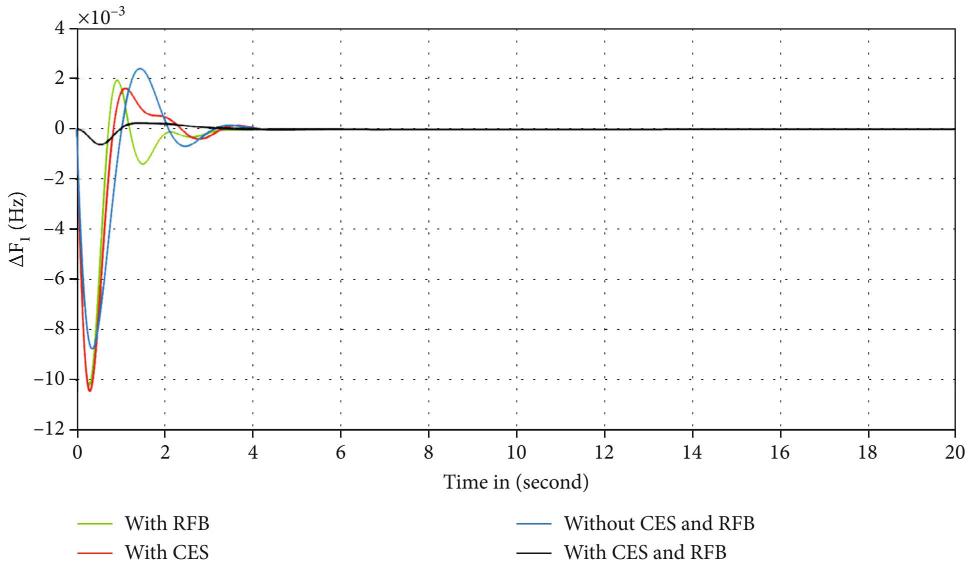

(a)

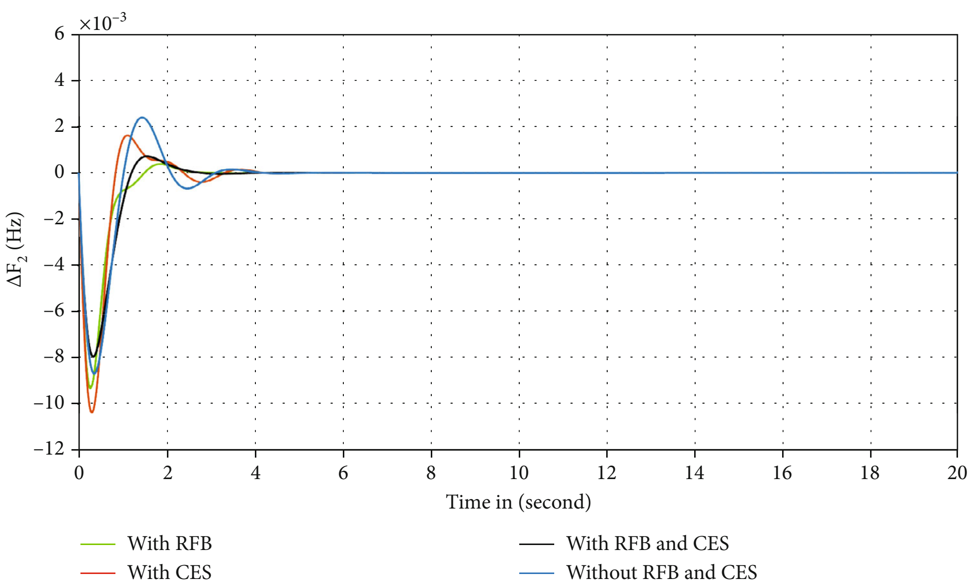

(b)

Figure 15: Continued.

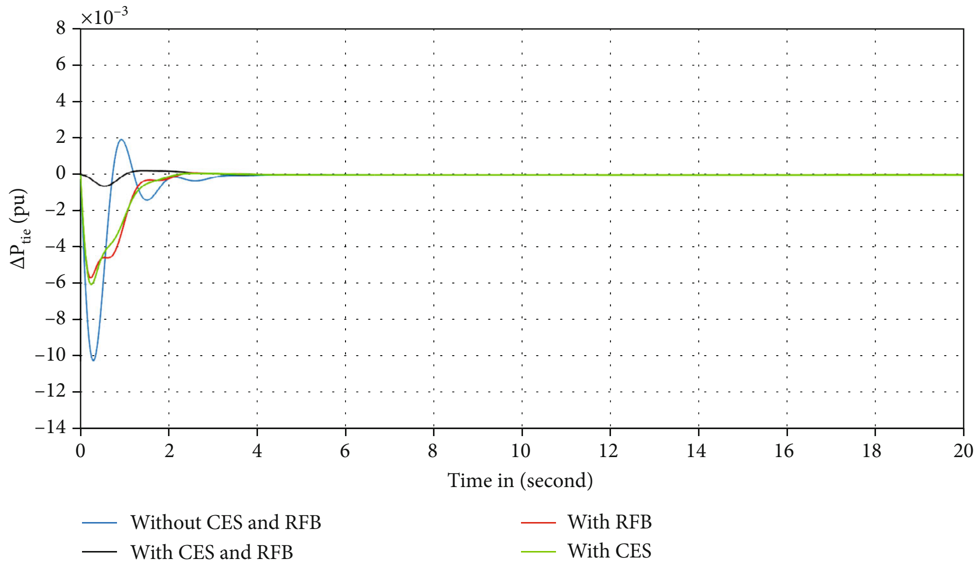

(c)

Figure 15: Transient response of PS considering case 3 for (a) ΔF_1, (b) ΔF_2, and (c) ΔP_{tie}.

Table 8: Comparison performance for case 3.

Transient parameters	System consideration	With CES and RFB	Without CES and RFB	With RFB	With CES
Time settling (Ts)	ΔF_1	2.88	4.00	3.96	3.65
	ΔF_2	2.60	4.33	2.93	4.05
	ΔP_{tie}	2.48	3.65	2.51	2.49
Overshoot (O_{sh})	ΔF_1	0.0002347	0.0024142	0.0019490	0.0016320
	ΔF_2	0.0007254	0.0024140	0.0003912	0.0017320
	ΔP_{tie}	0.000211	0.0019389	0.0001220	0.0000768
Undershoot (U_{sh})	ΔF_1	-0.0006158	-0.008772	-0.0102200	-0.010480
	ΔF_2	-0.008038	-0.008771	-0.0094160	-0.010490
	ΔP_{tie}	-0.000612	-0.0102192	-0.0056199	-0.006016

and PID controllers, the FOI-FOPIDD2 controller tuned using the SGO technique improved settling time for ΔP_{tie}, ΔF_2, and ΔF_1 by 19.11%, 17.34%, and 15.10%; 16.87%, 31.22%, and 25.07%; and 35.88%, 26.24%, and 23.89%. According to Table 7, the FOI-FOPIDD2 controller beat PIDD2 in terms of U_{sh} (69.44%, 71.23%, and 78.56%) and O_{sh} (56.21%, 67.90%, and 81.19%) for ΔF_1, ΔF_2, and ΔP_{tie}. Furthermore, as compared to a FOPID controller, the FOPIDD2 controller reduced overshoot by 57.89%, 67.98%, and 26.12%, respectively, for ΔF_1, ΔF_2, and ΔP_{tie}. Similarly, as compared to a PID controller, the FOI-FOPIDD2 controller considerably reduced undershoot by 31.78%, 68.46%, and 73.55%, respectively, for ΔF_1, ΔF_2, and ΔP_{tie}. Furthermore, Table 7 shows that the proposed FOPIDD2 controller outperforms PIDD2, PID, FOPID, and FOPI-PDF [25] and I-TD [52] approaches for change in area 2 (ΔF_2), variation in interconnected tie line (ΔP_{tie}), and change in area 1 (ΔF_1). As a result, the proposed FOI-FOPIDD2 controller appears to be a potential solution for increasing the load frequency performance in a variety of power systems. The controller efforts for area 1 and area 2 have been given in Figures 10 and 11, respectively, which show that our proposed controller performs well as compared to other controllers in respect of quicker settling, reduced overshoot, and undershoot. The convergence diagram for various controllers optimized with SGO is shown in Figure 12. From Figure 12, it can be observed that our proposed control strategies with SGO algorithm converge quickly as compared to other controllers.

Figures 13 and 14 present power output plots of nuclear (ΔP_N), thermal (ΔP_T), gas (ΔP_G), hydro (ΔP_H), and total power generation (ΔP_S) control regions in response to a 0.05 p.u. MW instantaneous demand disturbance in area 1. The graphs demonstrate the ultimate variations in power generation in area 1; ΔP_{G1}, ΔP_{H1}, ΔP_{N1}, ΔP_{T1}, and ΔP_{S1} are settled to 0.016 p.u. MW, 0.0135 p.u. MW, 0.006 p.u. MW,

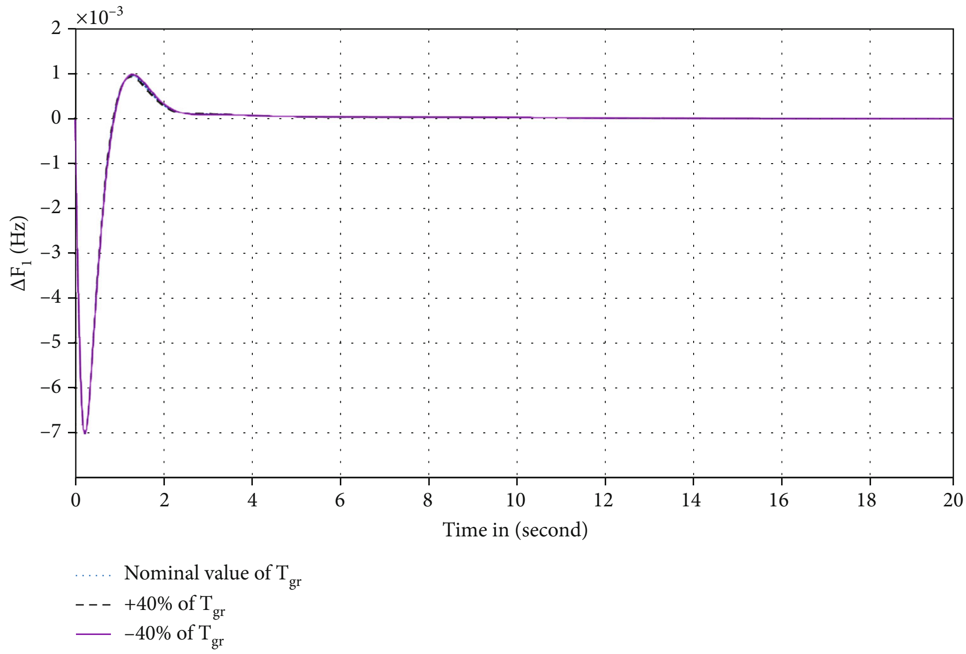

FIGURE 16: Variation of T_{gr} power system parameters for ΔF_1.

TABLE 9: Variations in PS parameters.

Transient response	Parameters of PS	% variation	ΔF_1	ΔF_2	ΔP_{tie}
Overshoot	T_{gr}	+40%	0.00023470	0.0004376	0.0001233
		-40%	0.0002360	0.0004398	0.0001298
	T_{rh}	+40%	0.0002201	0.0003407	0.0007254
		-40%	0.0002226	0.0003467	0.0007294
	T_{re}	+40%	0.0003508	0.0003834	0.0017100
		-40%	0.0003569	0.0003785	0.0017600
Undershoot	T_{gr}	+40%	-0.0006158	-0.0008692	-0.006016
		-40%	-0.000662	-0.000884	-0.006001
	T_{rh}	+40%	-0.000268	-0.000351	-0.000622
		-40%	-0.000220	-0.000392	-0.000583
	T_{re}	+40%	-0.006016	-0.005648	-0.008030
		-40%	-0.006080	-0.005690	-0.008090
Time settling	T_{gr}	+40%	2.69	2.86	3.29
		-40%	2.61	2.93	3.23
	T_{rh}	+40%	3.20	3.66	3.66
		-40%	3.22	3.83	3.68
	T_{re}	+40%	2.52	2.64	2.78
		-40%	2.81	2.63	2.80

0.0135 p.u. MW, and 0.05 p.u. MW, respectively. In area 2, these variations were eventually reduced to 0.00 p.u. MW.

5.3. Case 3 (Analysis of Redox Flow Battery and Capacitive Energy Storage). In case 3, the proposed SGO-FOI-FOPIDD2 has been tested with and without the presence of redox flow battery and capacitive energy storage. The results for ΔF_1, ΔF_2, and ΔP_{tie} are shown in Figures 15(a)–15(c) and Table 8. Figures 15(a)–15(c) demonstrate that our proposed SGO-FOI-FOPIDD2-based CES and RFB perform superiorly in respect of less overshoot, undershoot, and quicker settling time for area 1 ($O_{sh} = 0.00211$, $U_{sh} = -0.00062$, $Ts = 2.48$), area 2 ($O_{sh} = 0.00072454$, $U_{sh} = -0.00080$, $Ts = 2.60$), and tie line ($O_{sh} = 0.0002347$,

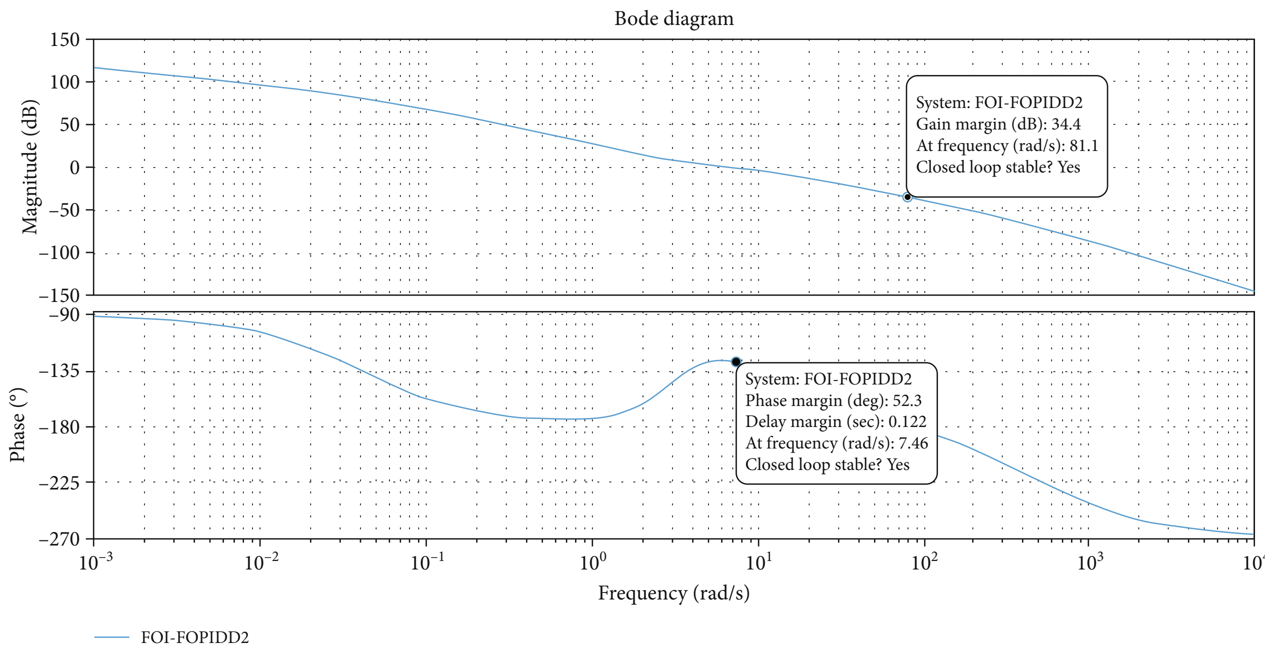

Figure 17: Bode diagram for the proposed system.

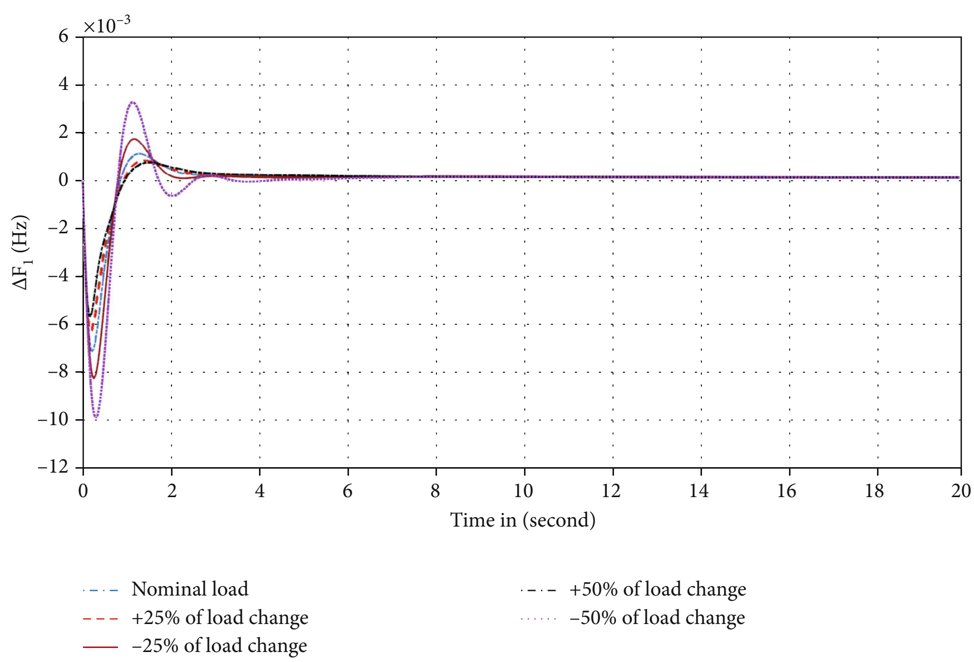

Figure 18: Load changes for ΔF_1.

$U_{sh} = -0.000615$, $Ts = 2.88$) as compared to SGO-FOI-FOPIDD2 based without CES and RFB for area 1 ($O_{sh} = 0.0019389$, $U_{sh} = -0.0102192$, $Ts = 3.65$), area 2 ($O_{sh} = 0.0024140$, $U_{sh} = -0.008771$, $Ts = 4.33$), and tie line ($O_{sh} = 0.0024142$, $U_{sh} = -0.008772$, $Ts = 4.00$); SGO-FOPIDD2-based CES for area 1 ($O_{sh} = 0.000768$, $U_{sh} = -0.00601$, $Ts = 2.49$), area 2 ($O_{sh} = 0.0017320$, $U_{sh} = -0.01049$, $Ts = 4.05$), and tie line ($O_{sh} = 0.0016320$, $U_{sh} = -0.010480$, $Ts = 3.65$); and SGO-FOI-FOPIDD2-based RFB for area 1 ($O_{sh} = 0.0001220$, $U_{sh} = -0.0056199$, $Ts = 2.51$), area 2 ($O_{sh} = 0.0003912$, $U_{sh} = -0.009416$, $Ts = 2.93$), and tie line ($O_{sh} = 0.0019490$, $U_{sh} = -0.01022$, $Ts = 3.96$). Using Figures 15(a)–15(c), we can see that the system's response to RFB and CES unit effects is better than its response without RFB and CES component effects in respect of O_{sh}, U_{sh}, and Ts. Additionally, Table 8 highlights the phenomenal results obtained by combining RFB and CES in our proposed method.

5.4. Case 4 (Sensitivity and Stability Analysis). Sensitivity analysis has been employed to examine the sturdiness of the recommended SGO-FOI-FOPIDD2 controller. The system's stability may occasionally be negotiated if the proposed control scheme is incapable of accommodating system parameter fluctuations. Various metrics for parameters like T_{gr}, T_{re}, and T_{rh} have been adjusted by approximately ±40% and then contrasted with their nominal parameter response to validate the robustness of the proposed controller. Figures 16 and Table 9 illustrate the dependability of the suggested controller when constraint uncertainty manifests, based on the results obtained when system parameter variations were employed. Figure 17 represents the bode diagram for the proposed FOI-FOPIDD2 controller which confirms the stability of the system due to their positive gain margins and phase margin values. In order to pretend real-time conditions, the performance of the SGO-FOI-FOPIDD2 controller is validated under varied load disturbances up to ±25% and ±50%, as depicted in Figure 18. Numerous parameters respond near to their supposed values, as shown in Table 9, indicating that the suggested SGO-FOI-FOPIDD2 controller provides reliable performance over a spectrum of approximately ±40% of the system's characteristics. Furthermore, the optimal values of the proposed controller have no need to reset controller for a wide range of parameters if employed with the real values at stated value.

6. Conclusion

In this paper, the squid game optimizer-based FOI-FOPIDD2 approach is recommended for the frequency stabilization of diverse two-area power systems containing reheat thermal, gas, hydro, nuclear, redox flow battery, and capacitive energy storage. The superiority of the proposed approach is established by comparing the results with some recent approaches. In terms of settling times and peak under-/overshoots, the squid game optimizer-based FOI-FOPIDD2 approach provides substantially better results than firefly algorithm, grey wolf optimizer, jellyfish search optimization, and particle swarm optimization-tuned FOI-FOPIDD2 controllers. In terms of enhanced settling time, the squid game optimizer-based FOPIDD2 controller outperforms the squid game optimizer-based FOPID, PIDD2, and PID controllers by 19.11%, 17.34%, and 15.10%; 16.87%, 31.22%, and 25.07%; and 35.88%, 26.24%, and 23.89% for ΔF_1, ΔF_2, and ΔP_{tie}, respectively. Similarly, the proposed squid game optimizer algorithms also reduced peak overshoot as compared to grey wolf optimizer algorithm by 35.34%, 46.78%, and 76.89%; jellyfish search optimization algorithm by 34.76%, 77.22%, and 82.56%; and firefly algorithm by 82.67%, 89.23%, and 29.67% for ΔF_1, ΔF_2, and ΔP_{tie}, respectively. The proposed squid game optimizer algorithms also reduced peak undershoot as compared to jellyfish search optimization algorithm by 62.34%, 22.90%, and 45.76%; grey wolf optimizer algorithm by 56.23%, 84.90%, and 32.16%; particle swarm optimization algorithm by 67.98%, 29.30%, and 34.56%; and firefly algorithm by 78.39%, 59.13%, and 38.55% for ΔF_1, ΔF_2, and ΔP_{tie}, respectively. It is observed that the recommended squid game optimizer-based FOI-FOPIDD2 is robust and yields higher performance when the size of the load disturbance and system components are changed. In the future, the proposed control scheme and other advanced controllers will be designed and implemented for conventional as well as renewable energy resources.

Data Availability

The data used to support the findings of this study is included within the article.

Conflicts of Interest

The authors declare no conflict of interest.

Authors' Contributions

Conceptualization was carried out by Yidie Ye, Amil Daraz, and Salman AlQahtani. Data curation was performed by Irfan Khan. Formal analysis was participated by Amil Daraz, Abdul Basit, and Irfan Khan. Funding acquisition was provided by Salman AlQahtani. Investigation was carried out by Irfan Khan. Methodology was assisted by Yidie Ye and Irfan Khan. Software was provided by Amil Daraz. Supervision was contributed by Yidie Ye. Validation was performed by Yidie Ye, Abdul Basit, and Irfan Khan. Visualization was participated by Amil Daraz and Abdul Basit. Writing of the original draft was performed by Yidie Ye and Amil Daraz. Writing, reviewing, and editing were carried out by Yidie Ye, Amil Daraz, Abdul Basit, Irfan Khan, and Salman AlQahtani.

Acknowledgments

This work was supported by Research Supporting Project Number (RSPD2024R585), King Saud University, Riyadh, Saudi Arabia.

References

[1] K. Singh and Y. Arya, "Tidal turbine support in microgrid frequency regulation through novel cascade fuzzy-FOPID droop in de-loaded region," *ISA Transactions*, vol. 133, pp. 218–232, 2023.

[2] I. Nasiruddin, T. S. Bhatti, and N. Hakimuddin, "Automatic generation control in an interconnected power system incorporating diverse source power plants using bacteria foraging optimization technique," *Electric Power Components and Systems*, vol. 43, no. 2, pp. 189–199, 2015.

[3] K. Singh and Y. Arya, "Correction to: Jaya-ITDF control strategy based frequency regulation of multi microgrid utilizing energy stored in high voltage direct current-link capacitors," *Soft Computing*, vol. 27, no. 9, p. 5971, 2023.

[4] J. R. Nayak, B. Shaw, B. K. Sahu, and K. A. Naidu, "Application of optimized adaptive crow search algorithm based two degree of freedom optimal fuzzy PID controller for AGC system," *Engineering Science and Technology, an International Journal*, vol. 32, article 101061, 2022.

[5] A. Daraz, H. Alrajhi, A. Basit, A. R. Afzal, A. N. Alahmadi, and I. A. Khan, *Load frequency stabilization of distinct hybrid conventional and renewable power systems incorporated with electrical vehicles and capacitive energy storage*, Research Square, 2024, PREPRINT (Version 1).

[6] L. C. Saikia, J. Nanda, and S. Mishra, "Performance comparison of several classical controllers in AGC for multi-area interconnected thermal system," *International Journal of Electrical Power and Energy Systems*, vol. 33, no. 3, pp. 394–401, 2011.

[7] M. Khamies, G. Magdy, S. Kamel, and B. Khan, "Optimal model predictive and linear quadratic Gaussian control for frequency stability of power systems considering wind energy," *IEEE Access*, vol. 9, pp. 116453–116474, 2021.

[8] B. Dhanasekaran, S. Siddhan, and J. Kaliannan, "Ant colony optimization technique tuned controller for frequency regulation of single area nuclear power generating system," *Microprocess Microsyst*, vol. 73, article 102953, 2020.

[9] G. Magdy, G. Shabib, A. A. Elbaset, and Y. Mitani, "Optimized coordinated control of LFC and SMES to enhance frequency stability of a real multi-source power system considering high renewable energy penetration," *Protection and Control of Modern Power Systems*, vol. 3, no. 1, p. 39, 2018.

[10] G. N. Nguyen, K. Jagatheesan, A. S. Ashour, B. Anand, and N. Dey, "Ant colony optimization based load frequency control of multi-area interconnected thermal power system with governor dead-band nonlinearity," in *Smart Trends in Systems, Security and Sustainability*, pp. 157–167, Springer, Singapore, 2018.

[11] K. Jagatheesan, B. Anand, N. Dey, A. S. Ashour, and V. E. Balas, "Load frequency control of hydro-hydro system with fuzzy logic controller considering non-linearity," in *In Recent Developments and the New Direction in Soft-Computing Foundations and Applications*, pp. 307–318, Springer, Cham, Switzerland, 2018.

[12] W. Tasnin, L. C. Saikia, and M. Raju, "Deregulated AGC of multi-area system incorporating dish-Stirling solar thermal and geothermal power plants using fractional order cascade controller," *International Journal of Electrical Power & Energy Systems*, vol. 101, pp. 60–74, 2018.

[13] M. Sharma, S. Dhundhara, Y. Arya, and S. Prakash, "Frequency excursion mitigation strategy using a novel COA optimised fuzzy controller in wind integrated power systems," *IET Renewable Power Generation*, vol. 14, no. 19, pp. 4071–4085, 2020.

[14] X. Qi, J. Zheng, and F. Mei, "Model predictive control–based load-frequency regulation of grid-forming inverter–based power systems," *Frontiers in Energy Research*, vol. 10, article 932788, 2022.

[15] X. Lv, Y. Sun, Y. Wang, and V. Dinavahi, "Adaptive event-triggered load frequency control of multi-area power systems under networked environment via sliding mode control," *IEEE Access*, vol. 8, pp. 86585–86594, 2020.

[16] K. Jagatheesan, A. Baskaran, N. Dey, A. S. Ashour, and V. E. Balas, "Load frequency control of multi-area interconnected thermal power system: artificial intelligence-based approach," *International Journal of Automation and Control*, vol. 12, no. 1, pp. 126–152, 2018.

[17] X. Yu and K. Tomsovic, "Application of linear matrix inequalities for load frequency control with communication delays," *IEEE Transactions on Power Apparatus and Systems*, vol. 19, no. 3, pp. 1508–1515, 2004.

[18] A. M. Eltamaly, A. A. Zaki Diab, and A. G. Abo-Khalil, "Robust control based on h∞ and linear quadratic Gaussian of load frequency control of power systems integrated with wind energy system," in *In Control and Operation of Grid-Connected Wind Energy Systems*, pp. 73–86, Springer, Cham, Switzerland, 2021.

[19] X. Bu, W. Yu, L. Cui, Z. Hou, and Z. Chen, "Event-triggered data-driven load frequency control for multiarea power systems," *IEEE Transactions on Industrial Informatics*, vol. 18, no. 9, pp. 5982–5991, 2022.

[20] A. H. Yakout, H. Kotb, H. M. Hasanien, and K. M. Aboras, "Optimal fuzzy PIDF load frequency controller for hybrid microgrid system using marine predator algorithm," *IEEE Access*, vol. 9, pp. 54220–54232, 2021.

[21] D. Habib, "Optimal control of PID-FUZZY based on gravitational search algorithm for load frequency control," *International Journal of Engineering Research*, vol. V8, no. 5, pp. 50013–50022, 2019.

[22] T. Kerdphol, F. S. Rahman, Y. Mitani, M. Watanabe, and S. Kufeoglu, "Robust virtual inertia control of an islanded microgrid considering high penetration of renewable energy," *IEEE Access*, vol. 6, pp. 625–636, 2018.

[23] A. Daraz, S. A. Malik, A. Basit, S. Aslam, and G. Zhang, "Modified FOPID controller for frequency regulation of a hybrid interconnected system of conventional and renewable energy sources," *Fractal and Fractional*, vol. 7, no. 1, p. 89, 2023.

[24] Y. Arya, "A novel CFFOPI-FOPID controller for AGC performance enhancement of single and multi-area electric power systems," *ISA Transactions*, vol. 100, pp. 126–135, 2020.

[25] G. Zhang, A. Daraz, I. A. Khan, A. Basit, M. I. Khan, and M. Ullah, "Driver training based optimized fractional order PI-PDF controller for frequency stabilization of diverse hybrid power system," *Fractal and Fractional*, vol. 7, no. 4, p. 315, 2023.

[26] Y. Arya, "AGC performance enrichment of multi-source hydrothermal gas power systems using new optimized FOFPID controller and redox flow batteries," *Energy*, vol. 127, pp. 704–715, 2017.

[27] M. Bhuyan, D. C. Das, and A. K. Barik, "Proficient power control strategy for combined solar gas turbine-wind turbine generator-biodiesel generator based two area interconnected microgrid employed with DC link using Harris's hawk optimization optimised tilt-integral-derivative controller," *International Journal of Numerical Modelling*, vol. 35, no. 4, article e2991, 2022.

[28] Y. Arya, "AGC of PV-thermal and hydro-thermal power systems using CES and a new multi-stage FPIDF-(1+PI) controller," *Renewab Energy*, vol. 134, pp. 796–806, 2019.

[29] M. Bhuyan, D. C. Das, A. K. Barik, and S. C. Sahoo, "Performance assessment of novel solar thermal-based dual hybrid microgrid system using CBOA optimized cascaded PI-TID controller," in *IETE journal of research*, pp. 1–18, Taylor & Francis, 2022.

[30] T. H. Mohamed, G. Shabib, E. H. Abdelhameed, M. Khamies, and Y. Qudaih, "Load frequency control in single area system using model predictive control and linear quadratic Gaussian techniques," *International Journal of Electrical Energy*, vol. 3, no. 3, pp. 141–143, 2015.

[31] M. Raju, L. Saikia, and N. Sinha, "Automatic generation control of a multi-area system using ant lion optimizer algorithm based PID plus second order derivative controller,"

International Journal of Electrical Power & Energy Systems, vol. 80, pp. 52–63, 2016.

[32] S. Kumari, G. Shankar, and B. Das, "Integral-tilt-derivative controller based performance evaluation of load frequency control of deregulated power system," in *Modeling, Simulation and Optimization*, pp. 189–200, Springer, Singapore, 2021.

[33] A. Daraz, S. A. Malik, A. T. Azar, S. Aslam, T. Alkhalifah, and F. Alturise, "Optimized fractional order integral-tilt derivative controller for frequency regulation of interconnected diverse renewable energy resources," *IEEE Access*, vol. 10, pp. 43514–43527, 2022.

[34] M. Ahmed, G. Magdy, M. Khamies, and S. Kamel, "Modified TID controller for load frequency control of a two-area interconnected diverse-unit power system," *International Journal of Electrical Power & Energy Systems*, vol. 135, article 107528, 2022.

[35] A. D. Falehi and H. Torkaman, "Promoted supercapacitor control scheme based on robust fractional-order super-twisting sliding mode control for dynamic voltage restorer to enhance FRT and PQ capabilities of DFIG-based wind turbine," *Journal of Energy Storage*, vol. 42, article 102983, 2021.

[36] A. D. Falehi and M. Rafiee, "LVRT/HVRT capability enhancement of DFIG wind turbine using optimal design and control of novel PIλDμ-AMLI based DVR," *Sustainable Energy, Grids and Networks*, vol. 16, pp. 111–125, 2018.

[37] N. Hasan, I. Asaidan, M. Sajid, S. Khatoon, and S. Farooq, "Robust self tuned AGC controller for wind energy penetrated power system," *Ain Shams Engineering Journal*, vol. 13, no. 4, article 101663, 2022.

[38] E. M. Ahmed, A. Elmelegi, A. Shawky, M. Aly, W. Alhosaini, and E. A. Mohamed, "Frequency regulation of electric vehicle-penetrated power system using MPA-tuned new combined fractional order controllers," *IEEE Access*, vol. 9, pp. 107548–107565, 2021.

[39] M. Barkat, "Novel chaos game optimization tuned-fractional-order PID fractional-order PI controller for load–frequency control of interconnected power systems," *Protection and Control of Modern Power Systems*, vol. 7, no. 1, p. 16, 2022.

[40] S. Mishra, P. C. Nayak, R. C. Prusty, and S. Panda, "Modified multiverse optimizer technique-based two degree of freedom fuzzy PID controller for frequency control of microgrid systems with hydrogen aqua electrolyzer fuel cell unit," *Neural Computing and Applications*, vol. 34, no. 21, pp. 18805–18821, 2022.

[41] A. Daraz, S. A. Malik, H. Mokhlis, I. U. Haq, F. Zafar, and N. N. Mansor, "Improved-fitness dependent optimizer based FOI-PD controller for automatic generation control of multi-source interconnected power system in deregulated environment," *IEEE Access*, vol. 8, pp. 197757–197775, 2020.

[42] M. Aly, E. A. Mohsmed, A. M. Noman, E. M. Ahmed, F. F. M. El-Sousy, and M. Watanabe, "Optimized non-integer load frequency control scheme for interconnected microgrids in remote areas with high renewable energy and electric vehicle penetrations," *Mathematics*, vol. 11, no. 9, p. 2080, 2023.

[43] E. M. Ahmed, E. A. Mohamed, A. Elmelegi, M. Aly, and O. Elbaksawi, "Optimum modified fractional order controller for future electric vehicles and renewable energy-based interconnected power systems," *IEEE Access*, vol. 9, pp. 29993–30010, 2021.

[44] P. C. Nayak, B. P. Nayak, R. C. Prusty, and S. Panda, "Sunflower optimization based fractional order fuzzy PID controller for frequency regulation of solar-wind integrated power system with hydrogen aqua equalizer-fuel cell unit," in *Energy sources, part a: recovery, utilization, and environmental effects*, pp. 1–19, Taylor & Francis, 2021.

[45] A. Latif, S. M. S. Hussain, D. C. Das, and T. S. Ustun, "Optimum synthesis of a BOA optimized novel dual-stage PI − (1 + ID) controller for frequency response of a microgrid," *Energies*, vol. 13, no. 13, p. 3446, 2020.

[46] S. Vishnoi, S. Nikolovski, M. Raju, M. K. Kirar, A. S. Rana, and P. Kumar, "Frequency stabilization in an interconnected micro-grid using smell agent optimization algorithm-tuned classical controllers considering electric vehicles and wind turbines," *Energies*, vol. 16, no. 6, p. 2913, 2023.

[47] S. Priyadarshani, K. R. Subhashini, and J. K. Satapathy, "Pathfinder algorithm optimized fractional order tilt-integral-derivative (FOTID) controller for automatic generation control of multi-source power system," *Microsystem Technologies*, vol. 27, no. 1, pp. 23–35, 2021.

[48] S. Ranjan, D. C. Das, A. Latif, and N. Sinha, "Electric vehicles to renewable-three unequal areas-hybrid microgrid to contain system frequency using mine blast algorithm based control strategy," *International Journal of Systems Assurance Engineering and Management*, vol. 12, no. 5, pp. 961–975, 2021.

[49] P. Zhang, A. Daraz, S. A. Malik, C. Sun, A. Basit, and G. Zhang, "Multi-resolution based PID controller for frequency regulation of a hybrid power system with multiple interconnected systems," *Frontiers in Energy Research*, vol. 10, article 1109063, 2023.

[50] N. Hakimuddin, I. Nasiruddin, and T. S. Bhatti, "Generation-based automatic generation control with multisources power system using bacterial foraging algorithm," *Engineering Reports.*, vol. 2, no. 8, article e12191, 2020.

[51] R. K. Sahu, G. C. Sekhar, and S. Priyadarshani, "Differential evolution algorithm tuned tilt integral derivative controller with filter controller for automatic generation control," *Evolutionary Intelligence*, vol. 14, no. 1, pp. 5–20, 2021.

[52] S. Kumari and G. Shankar, "Novel application of integral-tilt-derivative controller for performance evaluation of load frequency control of interconnected power system," *IET Generation Transmission and Distribution*, vol. 12, no. 14, pp. 3550–3560, 2018.

[53] M. Azizi, M. Baghalzadeh Shishehgarkhaneh, M. Basiri, and R. C. Moehler, "Squid game optimizer (SGO): a novel metaheuristic algorithm," *Scientific Reports*, vol. 13, no. 1, p. 5373, 2023.

[54] N. Hakimuddin, I. Nasiruddin, T. S. Bhatti, and Y. Arya, "Optimal automatic generation control with hydro, thermal, gas, and wind power plants in 2-area interconnected power system," *Electric Power Components and Systems*, vol. 48, no. 6-7, pp. 558–571, 2020.

[55] T. Ali, S. A. Malik, A. Daraz, S. Aslam, and T. Alkhalifah, "Dandelion optimizer-based combined automatic voltage regulation and load frequency control in a multi-area, multi-source interconnected power system with nonlinearities," *Energies*, vol. 15, no. 22, p. 8499, 2022.

[56] R. Hasan, M. S. Masud, N. Haque, and M. R. Abdussami, "Frequency control of nuclear-renewable hybrid energy systems using optimal PID and FOPID controllers," *Heliyon*, vol. 8, 2022.

[57] R. Choudhary, J. N. Rai, and Y. Arya, "Cascade FOPI-FOPTID controller with energy storage devices for AGC performance advancement of electric power systems," *Sustainable Energy*

Technologies and Assessments, vol. 53, no. Part C, article 102671, p. 102671, 2022.

[58] R. Choudhary, J. N. Rai, and Y. Arya, "FOPTID+1 controller with capacitive energy storage for AGC performance enrichment of multi-source electric power systems," *Electric Power Systems Research*, vol. 221, article 109450, 2023.

[59] S. Dhundhara and Y. P. Verma, "Capacitive energy storage with optimized controller for frequency regulation in realistic multisource deregulated power system," *Energy*, vol. 147, pp. 1108–1128, 2018.

[60] S. Rangi, S. Jain, and Y. Arya, "Utilization of energy storage devices with optimal controller for multi-area hydro-hydro power system under deregulated environment," *Sustainab Energy Technolo Assessments*, vol. 52, article 102191, 2022.

[61] M. Sharma, S. Dhundhara, Y. Arya, and S. Prakash, "Frequency stabilization in deregulated energy system using coordinated operation of fuzzy controller and redox flow battery," *International Journal of Energy Research*, vol. 45, no. 5, pp. 7457–7475, 2021.

[62] T. S. Gorripotu, R. K. Sahu, and S. Panda, "AGC of a multiarea power system under deregulated environment using redox flow batteries and interline power flow controller," *Engineering Science and Technology, an International Journal*, vol. 18, no. 4, pp. 555–578, 2015.

[63] G. Sharma, K. Narayanan, Y. Arya, and A. Panwar, "Impact of ultracapacitor and redox flow battery with JAYA optimization for frequency stabilization in linked photovoltaic-thermal system," *International Transactions on Electrical Energy Systems*, vol. 31, no. 5, article e12883, 2021.

[64] A. Darvish Falehi and H. Torkaman, "Robust fractional-order super-twisting sliding mode control to accurately regulatelithium-battery/super-capacitor hybrid energystorage system," *International Journal of Energy Research*, vol. 45, no. 13, pp. 18590–18612, 2021.

[65] A. D. Falehi, "Optimal power tracking of DFIG-based wind tur-bine using MOGWO-based fractional-order sliding mode controller," *Journal of Solar Energy Engineering*, vol. 142, no. 3, pp. 1–12, 2020.

[66] F. Zafar, S. A. Malik, T. Ali et al., "Metaheuristic optimization algorithm based cascaded control schemes for nonlinear ball and balancer system," *Processes*, vol. 12, p. 291, 2024.